Lanthanide transport, storage, and beyond: genes and processes contributing to XoxF function in *Methylorubrum extorquens* AM1

Paula Roszczenko-Jasińska,[a,£] Huong N. Vu,[b,*,£] Gabriel A. Subuyuj,[b,*] Ralph Valentine Crisostomo,[b,*] James Cai,[b] Charumathi Raghuraman,[b] Elena M. Ayala,[b] Erik J. Clippard,[b] Nicholas F. Lien,[b] Richard T. Ngo,[b] Fauna Yarza,[b,*] Caitlin A. Hoeber,[b] Norma C. Martinez-Gomez,[a]# Elizabeth Skovran[b]#

[a]Department of Microbiology and Molecular Genetics, Michigan State University, East Lansing, USA

[b]Department of Biological Sciences, San José State University, San José, California, USA

Running Head: Lanthanide transport and storage

[£] Both authors contributed equally and share first authorship

Address correspondence to: Elizabeth Skovran, elizabeth.skovran@sjsu.edu and N. Cecilia Martinez-Gomez, mart1754@msu.edu

* Present address: HNV: Department of Microbiology, University of Georgia, Athens, Georgia, USA; GAS: Department of Microbiology and Molecular Genetics, University of California at Davis, Davis, California, USA, RVC: Molecular Biology Institute, University of California at Los Angeles, Los Angeles, California, USA; FY: Department of Biochemistry and Biophysics, University of California at San Francisco, San Francisco, California, USA

ABSTRACT

Lanthanides are elements that have been recently recognized as "new life metals" in bacterial metabolism, yet much remains unknown regarding lanthanide acquisition, regulation, and use. The lanthanide-dependent methanol dehydrogenase XoxF produces formaldehyde, which is lethal to *Methylorubrum extorquens* AM1 if allowed to accumulate. This property enabled a transposon mutagenesis study to expand knowledge of the lanthanide-dependent metabolic network. Mutant strains were reconstructed and growth studies were conducted for over 40 strains detailing the involvement of 8 novel genes in lanthanide-dependent and independent methanol growth, including a fused ABC-transporter, aminopeptidase, LysR-type transcriptional regulator, putative homospermidine synthase, *mxaD* homolog (*xoxD*), porin family protein, and genes of unknown function previously published as *orf6* and *orf7*. Using genetic and biochemical analyses, strains lacking individual genes in the lanthanide transport cluster were characterized and named *lut* for **l**anthanide **u**tilization and **t**ransport (*META1_1778* to *META1_1787*). Consistent with previous reports, we corroborated that a TonB-ABC transport system is required for lanthanide transport to the cytoplasm. However, an additional outer membrane transport mechanism became apparent after longer growth incubations. Additionally, suppressor mutations that rescued growth of the ABC-transporter mutants were identified. Transcriptional reporter fusions were used to show that like iron transport, expression from the TonB-dependent receptor promoter, *lutH*, is repressed when lanthanides are in excess. Energy dispersive X-ray spectroscopy analysis was used to visualize the localization of lanthanum in wild-type and TonB-ABC transport mutant strains and showed for the first time, that *M. extorquens* AM1 stores cytoplasmic lanthanides in mineral form.

IMPORTANCE

Understanding the role of lanthanides in bacterial systems is an emergent field of study. Results from this work define mechanisms by which the methylotrophic bacterium, *M. extorquens* AM1, acquires and accumulates lanthanides. Lanthanides are critical metals for modern technologies and medical applications, yet lanthanide mining is cost-prohibitive and harmful to the environment. Methylotrophs are an attractive platform for the recovery of lanthanides from discarded electronics, mining leachate, and other waste streams as these microorganisms have been proven to sense and transport these metals for use in alcohol oxidation. Further, methylotrophs are effective biotechnological platforms for chemical productions and can use pollutants such as methane, and inexpensive feedstocks such as methanol. Defining the lanthanide acquisition, transport, and accumulation machinery is a step forward in designing a sustainable, clean platform to recover lanthanides in an efficient and less environmentally destructive manner.

INTRODUCTION

Lanthanide metals (Ln) impact the metabolism of many Gram-negative methylotrophic bacteria at both catalytic and transcriptional levels (1–3). Diverse types of pyrroloquinoline quinone (PQQ)-containing alcohol dehydrogenases (ADHs), specifically from the XoxF- and ExaF-families, have been shown to coordinate Ln in the active site (4–9) where they act as potent Lewis acids to facilitate a hydride transfer from the alcohol to PQQ, prompting alcohol oxidation (7, 10, 11). Some XoxF-methanol dehydrogenases (MeDHs) catalyze sequential oxidations to produce formate from methanol (12, 13), while formaldehyde is the product of other XoxF-MeDHs (8). Though much progress has been made regarding the catalytic role of Ln in ADH reactions, relatively little is known about how these Ln are acquired and incorporated into the enzymes that use them, and if they are stored intracellularly.

The role of Ln in metabolism is not exclusively catalytic. When Ln are transported into the cell, a transcriptional response occurs; this effect is commonly referred to as "the Ln-switch" or "rare earth-switch" (14–17). During the Ln-switch, the *mxa* operon is downregulated and transcript levels of the *xox* operon are upregulated (8, 15–19). In *M. extorquens* strains AM1 and PA1, the MxbDM two-component system and *xoxF* have been shown to be required for expression of the *mxa* genes and repression of the *xox* genes in the absence of Ln (20–22). However, suppressor mutations in the *mxbD* sensor kinase can arise which bypass the need for XoxF, presumably by constitutively activating the MxbM response regulator (3, 21, 22).

The machinery necessary for Ln transport is in the early stages of characterization and is predicted to be analogous to siderophore-mediated iron transport (22, 23). In *M. extorquens* AM1, ten genes predicted to be involved in Ln transport and utilization are clustered together in the genome (*META1_1778 – META1_1787*) and encode a TonB-dependent receptor, an ABC-

type transporter, four exported proteins of unknown function, lanmodulin which binds Ln, and an additional periplasmic-binding protein capable of Ln binding (*META1_1781*) (23, 24). TonB-dependent receptors are commonly used for the transport of metal ions such as iron (Fe^{3+}) and nickel (Ni^{2+}) that form poorly soluble salts under physiological conditions (25, 26). To facilitate the uptake of insoluble Fe^{3+}, these receptors have high affinity for metal-siderophore complexes. Siderophores are small molecules (hydroxamates, catecholates, and carboxylates) that are excreted by many bacteria and fungi to chelate insoluble metals (27–29). TonB is anchored in the inner membrane and spans the periplasmic space to interact with TonB-dependent receptors in the outer membrane. Once the siderophore-Fe^{3+} complex binds to the TonB-dependent receptor, it is transported through the receptor into the periplasm using the proton motive force harnessed by the TonB-ExbB-ExbD energy transducing system (30–32). In the periplasm, the siderophore-Fe^{3+} complex binds to a periplasmic binding protein that facilitates its interaction with an ABC-type transporter to translocate the siderophore-bound Fe^{3+} to the cytoplasm (33, 34). Iron release from the siderophore complex involves a reduction of Fe^{3+} to Fe^{2+}.

In *M. extorquens* strain PA1, genetic studies disrupting either the TonB-dependent receptor or deletions spanning multiple genes in the Ln transport cluster showed the requirement of some but not all genes in this cluster for Ln-dependent methanol growth (22). Accordingly, Mattocks et al. identified homologs of this system in *M. extorquens* AM1 and showed that a putative exported protein encoded by *META1_1781* can efficiently bind Ln from lanthanum (La^{3+}) to gadolinium. Additionally, they showed that the periplasmic binding component of the ABC transporter encoded by *META1_1778* was unable to bind Ln (23), possibly because it instead binds the predicted siderophore-like molecule necessary to transport Ln into the cell.

Currently, the regulation of the Ln-transport cluster genes is not understood. Iron transport is highly regulated as Fe^{2+} excess can promote Fenton chemistry and lead to the production of highly reactive radicals, which damage DNA, proteins, and other biomolecules (35). In bacteria such as *Escherichia coli*, the ferric uptake regulator (Fur) and the small RNA, *rhyB*, help to mediate iron homeostasis. When Fe^{2+} accumulates, Fur binds to iron uptake operons including *fecABCDE* (36), *fhuACDB* (37), *cirA* (38), *tonB* (39) and *exbB-exbD* (37) to repress iron transport and prevent oxidative stress. Herein, we show that like the iron paradigm, expression from the Ln TonB-dependent receptor is repressed by Ln when they are in excess.

In this study, we describe new pieces necessary to complete the Ln puzzle: the identification of novel transcriptional regulators and genes of unknown function, and the discovery and visualization of Ln storage in *M. extorquens* AM1. Growth phenotypes are reported for over 40 strains in methanol media containing and lacking Ln and reveal requirements for novel genes in both Ln-dependent and Ln-independent methanol growth. A detailed phenotypic characterization for strains lacking each component of the first 8 genes in the Ln transport cluster is described, including the ability of these strains to mutate or acclimate to allow Ln transport through a predicted secondary mechanism. Ln uptake was also quantified for several transport mutant strains. Finally, we show that *M. extorquens* AM1 not only incorporates Ln into the cytoplasm, but also stores Ln as crystalline cytoplasmic deposits. To our knowledge, this is the first demonstration of this behavior by a methylotrophic microorganism known to use Ln for metabolism.

RESULTS

XoxF produces formaldehyde *in vivo.* While XoxF can produce formate directly from methanol *in vitro*, XoxF contributes to formaldehyde production *in vivo* in *M. extorquens* AM1 (8). To expand these findings, strains lacking *fae* (encoding a formaldehyde-activating enzyme) and the different ADHs were constructed and tested for growth on solid La^{3+} medium containing both succinate and methanol as carbon sources (Fig. 1, Table 1). To confirm that loss of the Ca^{2+}-dependent MxaFI-MeDH does not affect growth of the *fae* mutant when Ln are present, an *fae mxaF* double deletion mutant strain was tested as a control. Loss of *xoxF1* alone allowed survival of the *fae* mutant strain, while additional loss of *xoxF2* allowed growth similar to the wild-type strain (Table 1). Loss of neither *exaF* nor *mxaF* conferred methanol resistance to the *fae* mutant strain, indicating that MxaFI and ExaF are not major contributors to formaldehyde production *in vivo* when Ln are present.

Identification of gene products that contribute to Ln-dependent methanol growth. A transposon mutagenesis study was designed to take advantage of the *in vivo* formaldehyde production capability of XoxF to identify genes required for Ln-dependent methanol oxidation. The strain used to conduct the mutant hunt contained a mutation in *mxaF* to make cells dependent on Ln for formaldehyde production, and a second mutation in *fae*, which would result in formaldehyde accumulation and death of the cells when methanol was provided as a substrate (Fig. 1). Transposon mutants with disruptions in genes involved in processes required for Ln-dependent methanol oxidation were selected for on medium containing succinate, methanol, La^{3+}, tetracycline (Tc), and rifamycin (Rif). Transposon insertions that reduced or eliminated formaldehyde production allowed survival and colony formation since methanol resistant strains

147 could use succinate for growth. In addition to genes required for methanol oxidation, this mutant
148 hunt had the potential to isolate insertions in an unknown formaldehyde transport system, which
149 would theoretically reduce formaldehyde levels in the cytoplasm (Fig. 1).
150 Over 600 transposon mutants were isolated, and their insertion locations mapped to the
151 *M. extorquens* AM1 genome. A variety of colony sizes were evident indicating that in some
152 mutants, formaldehyde production was eliminated while in others, it might only have been
153 reduced. Since it is likely that a portion of these transposon mutants became methanol-resistant
154 due to spontaneous second-site suppressor mutations and not a transposon insertion, only genes
155 that were identified three or more times were considered for further analysis and are listed in
156 Table 2. Among the genes identified were those with obvious roles in methanol oxidation such as
157 PQQ biosynthesis and the *xoxFGJ* genes. Three different clusters predicted to function in
158 cytochrome *c* biogenesis and heme export (*cyc* and *ccm* genes) (reviewed in (40)) were identified
159 along with insertions in an *mxaD* homolog gene (41). Insertions were isolated in six of the Ln
160 transport cluster genes including the ABC transporter components, the TonB-dependent receptor,
161 and two putative exported proteins (Fig. 2A). Notably, insertions were not isolated in Ln-binding
162 proteins, lanmodulin and *META1_1781* (23, 24). Additional genes of unknown function were
163 also discovered, including a LysR-type transcriptional regulator, a fused ABC transporter, a
164 porin family protein, a putative homospermidine synthase, a cytosol aminopeptidase, and *orf6*
165 and *orf7*, which are located downstream of the *pqqABCDE* operon (42). Based upon the work
166 detailed within, we propose to name the Ln transport cluster genes as *lut* for **l**anthanide
167 **u**tilization and **t**ransport (Fig. 2A).
168

Identification of novel components involved in methanol growth independent of Ln. To assess if the identified genes are specifically involved in Ln-dependent methanol oxidation or general methanol oxidation, 24 genes were chosen for reconstruction in *mxaF* and/or wild-type strain backgrounds. Methanol growth was assessed in the presence and absence of La^{3+} for all strains. As expected, deletion of genes in either of the two *pqq* biosynthesis operons (Δ*pqqBCDE*; Δ*pqqF*) eliminated Ln-dependent and independent methanol growth as did mutations in each of the three identified cytochrome *c* biogenesis and heme export clusters: *cycK*, heme lyase; *ccmB*, heme exporter; and *ccmC*, heme exporter (Table 3).

Novel genes affecting methanol metabolism were identified (Table 3). First, a fused ABC-type transporter (*META1_2359*) mutant was unable to grow in methanol medium with or without La^{3+}. After 85-100 h, second site suppressor mutations arose that allowed the strain to grow to similar culture densities as the wild-type strain but at a reduced growth rate. Second, *META1_3908* encodes a putative leucyl aminopeptidase that shares 38% identity and 57% similarity with PepA from *E. coli* MG1655. Loss of *META1_3908* resulted in a long growth lag (24 h without La^{3+}; 15 h with La^{3+}) and an approximate 60% decrease in growth rate in both conditions. The aminopeptidase appears to be in an operon based on overlap with *META1_3909*, a putative membrane protein of unknown function. Deletion of *META1_3909* did not result in a growth defect in methanol media with or without La^{3+} (data not shown). Third, loss of *hss* (*META1_2024*) encoding a putative homospermidine synthase resulted in a relatively short lag and an approximate 35% reduction in growth rate in methanol medium containing or lacking La^{3+}. Finally, while a LysR-type regulator (*META1_0863*) was hit nine times in the transposon mutagenesis study, loss of this LysR-type regulator only resulted in an approximate 10% decrease in growth rate in liquid methanol media. However, on solid methanol media, loss of

192 *META1_0863* had a more pronounced defect with colonies half the size of wild type (data not
193 shown).
194
195 **Identified genes specific to Ln-dependent methanol growth.** It was previously shown that
196 *xoxF* is required for growth in methanol medium that lacks Ln as XoxF is required for expression
197 of the MxaFI-MeDH (14, 21). Deletions were constructed in the *xoxG* and *xoxJ* genes to confirm
198 that *xoxGJ* are required for La^{3+}-dependent, but not La^{3+}-independent methanol growth in *M.*
199 *extorquens* AM1 as recently shown for *M. extorquens* PA1 (22). In the absence of La^{3+}, loss of
200 *xoxG* resulted in a growth reduction of 21% when compared to wild-type growth, while the *xoxJ*
201 growth defect was subtle (7% reduction) but with a 21 h lag (Table 3.) However, in methanol
202 La^{3+} medium, loss of either *xoxG* or *xoxJ* was equivalent to loss of both *xoxF1* and *xoxF2*
203 indicating that XoxGJ are essential for XoxF-dependent methanol oxidation as suggested by
204 recent biochemical studies (43–45). Transcriptional reporter fusion studies to assess expression
205 from the *mxa* promoter using a fluorescent reporter confirmed that unlike *xoxF*, neither *xoxG* nor
206 *xoxJ* was required for expression of the *mxa* genes in succinate plus methanol medium (average
207 relative fluorescence units (RFU)/OD_{600}: wild type, 322.9 ± 62.5; *xoxF1 xoxF2*, 3.1 ± 1.3; *xoxG*,
208 313.9 ± 24.0; *xoxJ*, 512.5 ± 54.9) with the *xoxJ* mutant resulting in a 1.9-fold upregulation from
209 the *mxa* promoter. These data are consistent with XoxF presence, but not XoxF activity, being
210 required for expression of the *mxa* genes as reported for *M. extorquens* PA1 (22).

211 The MxaD homolog, *META1_1771*, shares 43% identity and 58% similarity to the *M.*
212 *extorquens* AM1 MxaD protein, which has been suggested to facilitate interactions (directly or
213 indirectly) between a MeDH and its cytochrome (41). Loss of the *mxaD* homolog did not cause a
214 growth defect in methanol medium lacking La^{3+} but displayed an ~30% reduction in growth rate

when La^{3+} was provided (Table 3). These data suggest an important but non-essential role for the MxaD homolog in Ln-dependent methanol oxidation.

Marker-less deletion strains lacking either *orf6* or *orf7* were constructed and methanol growth was assessed in the presence and absence of La^{3+}. In methanol medium with La^{3+}, growth of the *orf6* mutant strain mirrored that of the *xoxF1 xoxF2* double mutant while growth of the *orf7* mutant was faster and like that of the *xoxF1* single mutant (Table 3). Since these genes are downstream of the operon encoding the PQQ biosynthetic pathway (*pqqABCDE*), addition of PQQ was tested to see if it would rescue the growth defect seen for the *orf6* and *orf7* mutants. While 1 μM PQQ was able to rescue growth of the *pqqBCDE* and *pqqF* mutant strains, PQQ did not rescue growth of the *orf6* or *orf7* mutants (data not shown).

Finally, an outer membrane porin-like gene (*META1_5071*) was identified in the transposon mutant hunt. Insertions were constructed in wild-type and *mxaF* strain backgrounds and growth in the presence and absence of La^{3+} was assessed. A slight growth defect was observed in the wild-type background in methanol La^{3+} medium (~10% reduction). However, in the absence of *mxaF* when cells require Ln for growth, a further growth reduction was observed (~20% reduction) along with a growth lag of 21 h.

Genetic characterization of the lanthanide utilization and transport cluster. The increasing evidence that Ln-dependent enzymes are widely distributed among different microbial taxa and environments leads to the parallel question of how these elements are scavenged for use in living systems. Our transposon mutagenesis studies demonstrate that genes encoding homologs of the TonB- and ABC-dependent Fe^{3+} scavenging pathways play a role in methanol metabolism when Ln are present. In addition to the transport system homologs, two of the four putative exported

proteins were identified as important for Ln-dependent growth. To facilitate a detailed genetic characterization of this gene cluster (Fig. 2A), mutations in individual genes from *lutA* through *lutH* were constructed in wild-type and *mxaF* mutant backgrounds and tested for growth in the presence and absence of La^{3+} (Table 3, Fig. 2C, Fig. S1). Mutants lacking individual transport cluster genes (*lutABEFG*) were complemented by expressing the respective gene in pCM62 (46) and growth similar to the wild-type strain was restored in each case (data not shown).

In the absence of *mxaF*, *M. extorquens* AM1 must obtain Ln for methanol growth (14) thus providing a condition to assess gene requirements for Ln utilization. Loss of the putative exported proteins that were not hit in the transposon mutant hunt either did not result in a growth defect (*mxaF lutD*) or decreased the growth rate by ~30% (*mxaF lutC*) (Table 3, Fig. 2C). Complementation of *lutC* was not tested so it is formally possible that the decrease in growth rate was due to polarity onto *lutEFG*. However, the *lutC* mutation was constructed such that adequate space for a *rut* site required for Rho-dependent polarity is not present (Table S1). In the *mxaF* strain background, loss of the remaining *lut* genes encoding putative exported or periplasmic components resulted in a significant growth defect. Specifically, loss of *lutA* (periplasmic binding component of ABC transporter) and the downstream putative exported protein encoded by *lutB* resulted in a ~88% reduction in growth rate, while strains lacking *lutG* displayed an ~81% reduction in growth rate (Fig. 2C, Table 3). The growth observed for these strains was not identified as second-site suppression or acclimation in our tests. These data show that while the periplasmic components of the Ln transport cluster are important to facilitate Ln utilization and transport, they are either not essential or have redundancy. This non-essentiality is in contrast with the requirement for the ATPase and membrane components of the ABC transporter (LutE and LutF, respectively), and the TonB-dependent receptor (LutH). Loss of *lutE* or *lutF* in the

261 *mxaF* strain background did not allow growth (Fig. 2C). However, after ~200 h and 150 h
262 respectively, second-site suppressor mutations arose which facilitated growth albeit 88% slower
263 than that of the wild-type strain (Fig. S1, Table 4). The *mxaF lutE* and *mxaF lutF* strains retained
264 the ability to grow in methanol with La^{3+} after succinate passage, indicating a genotypic change.
265 In contrast, after 90-120 h, growth of the *mxaF lutH* strain occurred in only ~60% of the cultures
266 (Fig. S1, Table 4). If growth did occur, this strain could grow without a lag once inoculated into
267 fresh methanol La^{3+} medium and exhibited wild-type colony sizes on solid methanol medium
268 similar to the wild-type strain (data not shown). However, if the culture was instead first streaked
269 onto minimal succinate medium to obtain isolated colonies, then inoculated into or onto fresh
270 methanol La^{3+} media (liquid or solid), the strain lost the ability to grow indicating that the
271 original growth was due to acclimation, not suppressor mutations.

272 As reported by Ochsner et al. (22), loss of *lutH* alone did not result in a growth defect in
273 methanol La^{3+} medium consistent with the hypothesis that LutH is needed for transport of Ln
274 into the cell and lack of Ln transport through the outer membrane enables growth with methanol
275 via the Ca^{2+}-MxaFI MeDH. For all other strains disrupted in the *lut* gene cluster, growth with a
276 functional *mxaF* gene was similar to growth of strains lacking *mxaF* (Table 3). Intriguingly, loss
277 of the membrane and ATPase components of the ABC transporter eliminated growth in the wild-
278 type background (Fig. 2C, Table 4). However, suppressor mutations arose in the *lutE* and *lutF*
279 mutant strains after 75-91 h. A second transposon mutant hunt revealed that insertions which
280 restored the ability of the *lutE* mutant to grow on methanol La^{3+} medium mapped to the TonB-
281 dependent receptor, *lutH*, consistent with expression of *mxaF* when cells are unable to sense Ln.
282 These data suggest that Ln must enter the cytoplasm in order to upregulate expression of the *xox*
283 and *exaF* ADHs and that Ln uptake into the periplasmic space may be enough to repress *mxa*

284 expression. It is also possible that Ln must first enter the cytoplasm to be released from the
285 predicted siderophore-like molecule (recently termed, lanthanophore (47)) to be incorporated
286 into XoxF. One possibility does not exclude the other. These discoveries suggest new hypotheses
287 to be tested regarding the Ln-switch.
288
289 **Quantification of lanthanide uptake.** The Arsenazo dye-based assay (48) was used to quantify
290 La^{3+} levels in culture supernatants (spent media) from wild type; *lutA*, *lutE*, *lutF* (ABC
291 transporter); and *lutH* (TonB-dependent receptor) mutant strains during growth (Fig, 3A). Strains
292 were grown in methanol medium containing 2 µM La^{3+} and limiting succinate (3.75 mM) as
293 *lutA*, *lutE*, and *lutF* mutant strains are unable to grow or grow poorly with methanol as a sole
294 carbon source (Table 3). Under these conditions, no significant decreases in La^{3+} levels were
295 observed for any strain during early- to mid-exponential phase (OD_{600} = 0.4) (Fig. 3B). As
296 cultures continued to grow and succinate was likely depleted, significant differences in La^{3+}
297 levels became apparent. At an OD_{600} of ~0.7, the supernatants of wild-type cultures contained
298 1.0 ± 0.1 µM La^{3+} (Fig. 3B). Similar levels were measured for the *lutA*, *lutE*, and *lutF* mutant
299 strains (1.1 ± 0.1 µM La^{3+}) suggesting Ln are still transported through the outer membrane. The
300 *lutA*, *lutE*, *lutF* mutant strains were unable to grow to an OD higher than 0.68 (Fig. 3A), but after
301 8 h in stationary phase, the La^{3+} concentration in the supernatant continued to decrease to 0.7 ±
302 0.1 µM (data not shown). Levels of La^{3+} in the supernatants from *lutH* mutants grown to the
303 same OD were significantly higher (1.5 ± 0.1 µM, Fig. 3B). Although a *lutH* mutant strain can
304 grow to a similar density as the wild-type strain, it is hypothesized that unlike wild type, the *lutH*
305 mutant grows using MxaFI for methanol consumption regardless of Ln presence, and therefore,
306 differences in La^{3+} levels in the supernatant are expected. In stationary phase, La^{3+} levels in the

supernatants from wild-type cultures were half of those found for the *lutH* mutant cultures (0.6 ± 0.1 µM and 1.3 ± 0.1 µM, respectively) (Fig. 3B). Decrease of La^{3+} in the *lutH* culture supernatants may reflect adsorption of La^{3+} onto the surface of the cells or interaction of La^{3+} with lipopolysaccharide, a phenomenon observed for other metals in different bacterial species (49). Additionally, the growth and acclimation data for the *mxaF lutH* strain suggests a secondary mechanism for Ln transport through the outer membrane (Table 3, Fig. S1).

Visualization of La^{3+} accumulation in *lut* transporter mutants. To further investigate the roles for the components of the TonB-ABC transport system, location of La^{3+} was assessed by transmission electron microscopy (TEM) in the *lutA*, *lutE*, *lutF*, *lutH* mutant strains. TEM coupled with energy dispersive X-ray spectroscopy (EDS) has been used to determine the elemental composition of cellular inclusions (50, 51) while La^{3+} has been widely used as an intracellular and periplasmic stain for electron microscopy (52–54). Here, we show that La^{3+} can be directly identified by TEM if accumulated inside *M. extorquens* AM1 cells. Strains were grown in methanol medium containing 20 µM La^{3+} and limiting succinate (3.75 mM). Samples with post-fixation by OsO_4 and staining with 2% uranyl acetate allowed the outer and inner membrane of the bacterial cells to be distinguished (Fig. 4A-E left subpanels), while visualization without fixation and staining enabled metal content analysis by removing the interaction between Os^{8+} and phosphate, which interferes with La^{3+} measurements (Fig. 4A-E right subpanels). Mutants lacking the TonB-dependent receptor (*lutH*) did not display La^{3+} deposits (Fig. 4A). In contrast, localized La^{3+} deposits were visualized in the periplasmic space in mutant strains lacking the ABC-transporter components (*lutA, lutE*, and *lutF*) as shown in Fig. 4B-E. EDS microanalyses confirmed these electron dense periplasmic deposition areas contained

330 La^{3+} (Fig. 4F). Electron-dense deposits were also observed in the cytoplasm from wild-type cells
331 grown with exogenous La^{3+} (Fig 4G). Taken together, these directly demonstrate the
332 requirements for the TonB-dependent receptor and ABC transporter in Ln transport.
333
334 **Expression of *lutH* is repressed by La^{3+}.** To test if expression of the of Ln uptake genes is
335 regulated in a similar manner to Fe^{3+} uptake genes, a fluorescent transcriptional reporter fusion
336 was used to monitor expression from the *lutH* promoter in methanol media. Addition of
337 exogenous La^{3+} repressed expression 4-fold (RFU/OD_{600} = 210 ± 7 without La^{3+}; RFU/OD_{600} =
338 47 ± 5 with La^{3+}) suggesting that when Ln are in excess, transport is down-regulated. This is
339 consistent with the mechanism of control for iron homeostasis (37, 39).
340
341 **Ln are stored as cytoplasmic crystalline deposits.** To determine if *M. extorquens* AM1 stores
342 Ln, an *mxaF* mutant was grown in methanol medium with 10-times the standard concentration of
343 La^{3+} (20 µM $LaCl_3$) resulting in a growth rate of 0.15 ± 0.00 h^{-1}. Six hours post stationary phase,
344 cells were washed four times and sub-cultured into methanol medium lacking La^{3+} using Ln-
345 depleted tubes (14). To ensure growth was not due to contamination, strains were streaked onto
346 methanol solid medium without La^{3+}. As shown in Fig. 5, a similar growth rate to that observed
347 in the presence of La^{3+} was obtained (subculture #1, 0.16 ± 0.00 h^{-1}) until the culture reached an
348 OD_{600} of ~1.0. A slower growth rate was noted as growth continued to an OD of ~1.5. This
349 culture was then washed and sub-cultured into fresh methanol medium lacking Ln as described
350 above. Cells continued to grow but at a very impaired rate (0.01 ± 0.0 h^{-1}) until they reached a
351 peak OD of ~1.3. The use of Ln-depleted glassware reduces Ln levels such that growth of an
352 *mxaF* mutant strain appears negligible for 100 h when grown in media lacking Ln (14). As these

storage growth curves were carried out for >600 h, a control experiment was done to determine growth due to either background levels of non-MxaF ADH activity or due to leeching of residual Ln from the glassware. Growth of an *mxaF* mutant strain that had not been previously grown with Ln had slower growth than subculture #2 with a growth rate of 0.003 ± 0.000 h^{-1} (data not shown).

To visualize Ln storage within the cell, cultures of the wild-type strain were grown in the presence and absence of 20 µM $LaCl_3$, harvested at mid-exponential phase, and immediately fixed with glutaraldehyde. Samples without post-fixation and staining were analyzed for both visualization and metal content. Electron-dense deposits were observed in the cytoplasm from cells grown with exogenous La^{3+} (Fig. 6A-B). Samples were analyzed using EDS and corroborated that the dense deposits contained La^{3+} (Fig. 6C). When grown without La^{3+}, only a few cells showed smaller electron dense areas (Fig. 6E-F); however, EDS analysis did not detect La^{3+} in these cases (Fig. 6G). These data demonstrate that La^{3+} can be stored in *M. extorquens* as metal deposits. Moreover, EDS analysis of electron dense areas from the wild-type strain grown with La^{3+} (Fig S2) determined a content of La ($22.2 \pm 1.0\%$), P ($15.1 \pm 2.1\%$), and oxygen (O) ($51.1 \pm 1.9\%$) suggesting Ln are complexed with phosphate. Traces of chloride (3.0%), calcium (2.2%), and aluminum (3.4%) ions were also detected. The copper, carbon, and silicon ion content from the support grids and embedding medium were not considered for metal content calculations. High-resolution transmission electron microscopy (HRTEM) images of the La deposits showed an atomic lattice (Moire fringes/pattern) indicating a crystalline nature (Fig. 6D). These results suggest that La is embedded in inorganic phosphate crystals which form the electron dense deposits observed in the cytoplasm.

DISCUSSION

The Ln-dependent XoxF-MeDH has been shown to produce formaldehyde *in vivo* (8). Here we show that formaldehyde accumulation due to disruption of *fae* is lethal when tested on methanol and La^{3+} solid medium, which enabled a genetic selection to identify genes required for or involved in methanol oxidation by XoxF. Additionally, our phenotypic data are consistent with *in vitro* and *in vivo* work that suggests formate is the product of ExaF-mediated methanol oxidation (5, 8) and with our previous work that shows expression from the *mxa* promoter is repressed when Ln are present (8, 14).

The mutational analysis presented expands the identification of gene products contributing to methanol metabolism, Ln transport and utilization, and the characterization of genes with known or predicted roles in Ln metabolism. Using growth and transcriptional reporter fusion studies, we show that unlike *xoxF*, *xoxG* and *xoxJ* are not required for expression of the *mxa* genes but are likely required for XoxF activity as loss of either *xoxG* or *xoxJ* resulted in growth that mirrored the *xoxF1 xoxF2* double mutant strain. Recent biochemical and structural analyses of XoxG suggest that this cytochrome is tuned specifically for light Ln, while XoxJ interacts with and may activate XoxF (44). In the methanotroph *Methylomonas* sp. strain LW13, loss of *xoxG* also results in a growth defect in methanol medium lacking Ln, suggesting an unknown role in metabolism in addition to functioning as a cytochrome for XoxF-mediated methanol oxidation (43). Our studies are consistent with an unknown role for XoxGJ in *M. extorquens* AM1 as strains lacking *xoxG* or *xoxJ* display a growth lag or reduction in growth rate. These data are in contrast to previous reports for *M. extorquens* PA1 and AM1, where loss of *xoxGJ* did not result in a growth phenotype in methanol medium lacking Ln (22, 42). Notably,

397 the previous AM1 studies were carried out on agar plates where subtle growth defects may not
398 be apparent and both published studies were conducted using a different growth medium.
399 Our transposon mutagenesis and growth studies lay the foundation for future work
400 characterizing the roles for new methylotrophic gene products. A fused ABC-transporter
401 (*META1_2359*) was found to be essential for methanol growth independent of Ln presence.
402 Some possible functions for META1_2359 may include formaldehyde transport or PQQ export
403 into the periplasm for incorporation into the ADHs. Leucyl aminopeptidases like *META1_3908*
404 are often involved in protein processing or turnover, yet some have been shown to exhibit DNA
405 binding activity and facilitate regulation or site-specific recombination (55). Homospermidine
406 synthases (*hss*) function in polyamine biosynthesis and their products (e.g. putrescine,
407 spermidine) and have been implicated in roles as diverse as host pathogen interactions, biofilm
408 formation, siderophore production, acid resistance, and free radical scavenging (56, 57). LysR-
409 type regulators are members of a large family of transcriptional regulators that can be both
410 activators and repressors of a wide variety of genes involved in diverse cellular processes (58).
411 More work is required to identify specific roles for these genes in the metabolism of *M.*
412 *extorquens* AM1.
413 Loss of the *mxaD* homolog, *META1_1771*, resulted in a growth defect only if La^{3+} was
414 included in the medium. Based on its sequence similarity to MxaD, localization in the genome,
415 and growth phenotypes, we propose to name *META1_1771* as *xoxD*. Interestingly, upstream of
416 *xoxD* is another *mxaD* homolog (*META1_1772*) and downstream is an *mxaE* homolog
417 (*META1_1770*). These genes were not identified in the transposon mutant hunt and were not
418 characterized in this study.

Before the existence of Ln-dependent MeDHs were known, mutations were constructed in *orf6* and *orf7* due to their proximity to C_1 genes and it was concluded that these genes likely did not have a role in C_1-metabolism as they grew on methanol medium in the absence of Ln (42). Results here clearly suggest that *orf6* and *orf7* are important for Ln-dependent methylotrophy and more work is needed to determine their specific roles.

Characterization of the *lut* operon is consistent with the observations recently reported for *M. extorquens* PA1 (22) where a TonB-ABC transport system contributes to Ln transport into the cytoplasm. It has been proposed that Ln may be acquired via lanthanophores (47), which enter through a TonB-dependent receptor (22, 23). It may be that secondary mechanisms exist to take up Ln chelated by phosphates or citrate, compounds which are present in *Methylobacterium* PIPES (MP) medium (59). It is possible that these complexes pass through the outer membrane via a porin, though that is speculation at this point. Of interest, *META1_5017* is a porin family protein that was identified in our transposon mutagenesis studies, and loss of this gene resulted in a 21 h lag and an approximate 20% reduction in growth rate only in the *mxaF* mutant background. This phenotype would be consistent with a reduction in Ln import. It may be that in the *lutH* mutant, non-siderophore bound Ln slowly enter through META1_5017 porin and once a threshold is reached, trigger expression and function of the Ln-dependent ADHs. This may explain the acclimation of the *mxaF lutH* strain after ~100 h but more work is needed to confirm this hypothesis. Since transposon mutants disrupted in the genes encoding lanmodulin or the Ln-binding protein downstream of lanmodulin were not isolated, our observations are consistent with the findings in *M. extorquens* PA1 that suggest a non-essential or redundant role for these genes in Ln metabolism (22). Notably, the *mxaF fae* transposon mutagenesis study did not identify obvious gene candidates for lanthanophore biosynthesis though over 600 insertions were

442 mapped to the genome. This may indicate that more than one lanthanophore is produced by the
443 cell or that the lanthanophore has an essential role that is not yet understood. Additionally, we
444 show that like the paradigm for regulation of siderophore mediated Fe^{3+} uptake, expression from
445 the TonB-dependent receptor promoter, *lutH*, is repressed by Ln.

446 Our transport, TEM, and EDS analyses are consistent with LutH facilitating Ln transport
447 into the periplasm and the ABC transport system facilitating Ln transport into the cytoplasm.
448 La^{3+} concentrations found in the supernatant from strain variants lacking transport system
449 components suggest that once in the periplasm, significant concentrations of La^{3+} do not go back
450 outside of the cell as ABC transporter mutants showed uptake of La^{3+} from the medium similar
451 to the wild-type strain. Intriguingly, TEM and EDS studies with ABC transporter mutant strains,
452 demonstrated localized accumulation of Ln in the periplasmic space. It is not yet clear how or
453 why Ln accumulate in specific areas rather than appear diffused throughout the periplasm. Taken
454 together, our phenotypic growth, transport, and visualization studies suggest that Ln must enter
455 the cytoplasm for the *xox* and *exaF* ADHs to be expressed and that Ln uptake into the
456 periplasmic space may be enough to repress *mxa* expression. This work will facilitate new
457 exploration of the Ln-switch.

458 It has been observed that bacteria such as *Bacillus licheniformis* (60), *Myxococcus*
459 *xanthus* (54), and *Pseudomonas aeruginosa* (61) can effectively adsorb La^{3+} in mineral form
460 onto their cell surface when Ln are at high concentrations (mM). Here, TEM and EDS analyses
461 demonstrate that *M. extorquens* AM1 stores Ln in the cytoplasm in crystal form. This is
462 consistent with recent studies for the non-methylotroph *Thermus scotoductus* SA-01 which
463 showed that Eu^{3+} can accumulate in the cytoplasm. However, these studies were conducted using
464 very high Eu^{3+} concentrations that are not typically found in nature (51). Further, a role for Eu^{3+}

in the metabolism of *T. scotoductus* SA-01 remains to be defined. For many bacteria, biomineralization is a mechanism used to cope with toxicity of different metals, manage waste products, sense and change orientations in accordance with geomagnetic fields, and store important cations for growth (62–67). It has been reported that some microorganisms store polyphosphate as volutin or metachromatic granules, and these granules are often complexed with cations like Mg^{2+} and Ca^{2+} (68–71). It is not yet known if *M. extorquens* AM1 stores Ln complexed to polyphosphate, however, the ratios of P, O, and La detected in our studies are consistent with Ln phosphates. Detailed studies are necessary to define the exact chemical structure of Ln storage deposits in *M. extorquens* AM1. Our current findings bring exciting implications for bacterial metabolism and cell biology, and for the development of bioremediation and biometallurgy strategies for Ln recovery.

MATERIALS AND METHODS

Bacterial strains and cultivation. Strains and plasmids used in this study are listed in Table S2. *E. coli* strains were cultivated in Lysogeny Broth (LB) medium (72) (BD, Franklin Lakes, NJ) at 37°C. *M. extorquens* AM1 strains were grown in *Methylobacterium* PIPES [piperazine-*N*,*N*'-bis(2-ethanesulfonic acid)] (MP) media (59) supplemented with succinate (15 mM) and/or methanol (125 mM) as described (14) unless otherwise stated. Conjugations took place on Difco Nutrient Agar (Thermo Fisher Scientific, Waltham, MA). Cultures were grown in round-bottom polypropylene or borosilicate glass culture tubes, or 250 mL polypropylene Erlenmeyer flasks (Thermo Fisher Scientific, Waltham, MA). If glass tubes or flasks were used to culture bacteria, they were pretreated to remove Ln as previously described (14). Liquid cultures were grown at 29°C and shaken at 200 and 180 rpm in Innova 2300 and Excella E25 shaking incubators (Eppendorf, Hamburg, Germany), respectively. $LaCl_3$ was supplemented to a final concentration of 2 or 20 μM when indicated. To prepare PQQ, methoxatin disodium salt (Santa Cruz Biotechnology, Dallas, Tx) was dissolved in deionized water at pH 12-13 and filter sterilized. When necessary, antibiotics were added at the following concentrations: rifamycin (Rif, 50 μg/mL), tetracycline (Tc, 10 μg/mL for LB, 5 μg/mL for MP or 10 μg/mL when used together with Rif), kanamycin (Km, 50 μg/mL), ampicillin (Ap, 50 μg/mL).

Plasmid and strain construction. Primers used for plasmid and strain construction are listed in Table S1. The allelic exchange plasmid pHV2 was constructed by cloning the *sacB* gene from pCM433 (73) into the PscI site of pCM184 (74) in the same orientation as the Tc resistant gene. Insertion and orientation of *sacB* was confirmed by colony PCR. The *lutH* transcriptional reporter fusion was constructed by cloning the promoter region of *lutH* into the AclI and EcoRI

499 sites upstream of a promoter-less *venus* gene in pAP5 (21). To create overexpression constructs
500 for complementation studies, individual genes in the *lut* operon (*lutA, lutB, lutE, lutF*, and *lutG)*
501 were cloned into the KpnI and SacI sites downstream of a P_{lac} promoter in pCM62 (46).
502 Diagnostic PCR was used to confirm successful integration of inserts. Plasmids were maintained
503 in *E. coli* TOP10 (Invitrogen, Carlsbad, CA).
504 Gene deletions were constructed using pCM184 or pHV2 as previously described (14)
505 except 5% sucrose was added for counter selection against single crossovers (73) when using
506 pHV2. Plasmids were conjugated into *M. extorquens* AM1 via biparental mating using *E. coli*
507 S17-1 (75) or triparental mating using *E. coli* TOP10 (Invitrogen, Carlsbad, CA) and *E. coli*
508 harboring the conjugative plasmid pRK2013 as described (14). When indicated, the Km
509 resistance cassette was resolved using pCM157 to achieve marker-less deletions (74).
510
511 **Transposon mutagenesis.** Suicide vector pCM639 carrying a mini transposon IS*phoA*/hah-Tc
512 (76) was conjugated into *mxaF fae* and *lutE* strain backgrounds via triparental mating as
513 described (14, 77). Dilutions of the mating mixtures were plated onto MP succinate (15 mM)
514 plus methanol (50 mM) La^{3+} medium for the *mxaF fae* strain background and MP methanol (125
515 mM) La^{3+} medium for the *lutE* strain background. Media contained 10 µg/mL Tc to select for
516 successful integration of the mini transposon into *M. extorquens* AM1 chromosome and 50
517 µg/mL Rif to counter select against *E. coli* strains bearing pCM639 or pRK2013. Plates were
518 incubated for 5-7 days at 29^{o}C. Transposon mutant colonies were streaked onto MP succinate
519 plus methanol La^{3+} Tc (*mxaF fae*) or MP methanol La^{3+} (*lutE*) medium for downstream studies.
520

Location of transposon insertions. To identify the transposon insertion sites, genomic DNA was isolated using Qiagen's DNeasy UltraClean microbial kit (Qiagen, Germantown, MD). Degenerate nested PCR was performed as described (77, 78) with the following exceptions: PCR reactions contained 1 µM of each primer, 0.05 U/µL Dream Taq (Thermo Fisher Scientific, Waltham, MA), and 5% dimethyl sulfoxide. Modifications to the PCR amplification parameters included 2 minutes for the initial denaturation at 95°C, 6 cycles of annealing at 40°C followed by 25 cycles of annealing at 65°C for the first PCR reaction, and 30 cycles of annealing at 65°C for the second PCR reaction. PCR products were purified using a Qiagen PCR purification kit (Germantown, MD). Sequence analysis was performed using TransMapper, a Python-based software developed in-house to identify transposon insertion locations and map them to the *M. extorquens* AM1 genome. Insertion locations were visualized using the SnapGene Viewer (GSL Biotech LLC, Chicago, IL).

Phenotypic analyses. Growth phenotypes were determined on solid or in liquid MP media using a minimum of three biological replicates. On solid media, colony size was scored after four days. Growth curve analysis was conducted at 29°C in an Excella E25 shaking incubator (New Brunswick Scientific, Edison, NJ) using a custom-built angled tube rack holder as previously described (14). Optical density (OD_{600}) was measured at 600 nm using a Spectronic 20D spectrophotometer (Milton Roy Company, Warminster, PA). For strains with extended growth lags, suppression and acclimation was assessed. Strains from the growth curves were streaked onto methanol La^{3+} medium after they reached stationary phase. If the parent stock strain did not grow on methanol La^{3+} and the strain post-growth curve grew, acclimation versus suppression was tested. Strains were passaged from the methanol medium plate to a succinate medium plate.

After colonies grew on succinate medium, they were streaked back onto methanol La^{3+} medium. If strains retained the ability to grow on methanol medium, it was concluded that growth was due to a suppressor mutation. If strains lost the ability to grow on methanol medium after succinate passage, it was concluded growth was due to acclimation and not a genetic change.

For Ln storage growth experiments, *mxaF* deletion strains were grown with 20 µM $LaCl_3$ until six hours after entrance into stationary phase. Cells were centrifuged and washed four times with MP medium lacking La^{3+} and a carbon source, and sub-cultured into fresh MP methanol medium without La^{3+}. Six hours post stationary phase, the cultures were streaked onto MP methanol medium with and without La^{3+} to check for contamination. Cultures were again washed and sub-cultured as described above. This process was repeated for two rounds of growth without La^{3+}.

Transcriptional reporter fusion assays. *M. extorquens* AM1 strains carrying *mxa* and *lutH* transcriptional reporter fusions (Table S2) which use *venus* (79) as a fluorescent reporter were grown in MP medium supplemented with methanol only or methanol and succinate with and without La^{3+} as indicated in the text. Expression was measured as relative fluorescent units (RFU) using a SpectraMax M2 plate reader (Molecular Devices, Sunnyvale, CA) and normalized to OD_{600} as previously described (14).

La^{3+} depletion during *M. extorquens* AM1 growth. Overnight cultures of wild type, *lutA*, *lutE*, *lutF*, and *lutH* mutant strains were inoculated 1:50 into 250 mL polycarbonate flasks (Corning Inc., Corning, NY) containing 75 mL of MP medium (59). Succinate (3.75 mM) and methanol (125 mM) were added as carbon sources with 2 µM $LaCl_3$. Flasks were incubated at 28°C at 200

567 rpm in Innova 2300 shaking incubators (Eppendorf, Hauppauge, NY) for 44 h. To monitor La^{3+}
568 depletion during *M. extorquens* AM1 cultivation, the Arsenazo III assay was used as previously
569 described (48). 5 mL samples were collected at 4 different time points (OD_{600} of 0.04, 0.4, 0.7,
570 and 1.5). The concentration of La^{3+} remaining in the supernatant was calculated using the
571 calibration curve prepared as previously described (48). A control of 3 uninoculated flasks
572 containing MP medium with 2 μM $LaCl_3$ were considered to determine La^{3+} adsorption by the
573 flasks which was subtracted from the culture measurements. The initial concentration of La^{3+} in
574 the media (before growth) was measured using the Arsenazo III assay in the same way as
575 described above. Significant differences between depletion of La^{3+} by different strains were
576 calculated using One-way ANOVA followed by a T-test.
577
578 **Cellular locations of Ln visualized using Transmission Electron Microscopy (TEM).** Sample
579 preparation for TEM: wild-type, *lutA*, *lutE*, *lutF*, and *lutH* mutant strains were grown in MP
580 medium containing 125 mM methanol and 3.75 mM succinate as carbon sources with or without
581 the addition of 20 μM $LaCl_3$ until they reached an OD of ~0.6. 3 mL of cells were harvested by
582 centrifugation for 3 min at 1500 × *g* at room temperature and fixed for 30 min in 1 mL of 2.5%
583 (v/v) glutaraldehyde (Electron Microscopy Sciences, Hatfield, PA) in 0.1 M cacodylate buffer
584 (Electron Microscopy Sciences, Hatfield, PA) at room temperature. After fixation, cells were
585 pelleted by centrifugation for 3 min at 1500 × *g* at room temperature and washed with 1 mL of
586 0.1 M cacodylate buffer. Cell pellets were embedded in 2% (w/v) agarose and washed three
587 times with 0.1 M cacodylate buffer. When indicated, pellets in agarose blocks were post-fixed
588 for 30 min in 1% osmium tetroxide in 0.1 M cacodylate buffer. Samples were washed three times
589 with 0.1 M cacodylate buffer, dehydrated in acetone, and embedded in Spurr resin (Electron

590 Microscopy Sciences, Hatfield, PA). Blocks were polymerized at 60ºC for 48 h. 70 nm sections
591 were obtained with a Power Tome XL ultramicrotome (RMC Boeckeler Instruments, Tucson
592 AZ), deposited on 200 mesh carbon coated grids and stained with 2% uranyl acetate (Electron
593 Microscopy Sciences, Hatfield, PA). To assess the presence of La^{3+} by EDS, sections were left
594 unstained. To image the distribution of cellular La, a TEM JOEL 1400 Flash (Japan Electron
595 Optics Laboratory, Japan) was used. Detection of La in the cells and high-resolution imaging
596 were done with a JEOL 2200FS (Japan Electron Optics Laboratory, Japan) operated at 200kV.
597 X-ray energy dispersive spectroscopy was performed using an Oxford Instruments INCA system
598 (Abingdon, United Kingdom).
599
600 **ACKNOWLEDGMENTS**
601 We would like to thank Dr. Lena Daumann and Dr. Nathan Good for critical review of this
602 manuscript. We would like to thank San José State University General Microbiology students
603 who isolated transposon mutants and purified genomic DNA for sequencing as part of a class
604 research project. The mutant hunt in this study was inspired by Dr. Elizabeth Skovran's
605 undergraduate research mentor, Dr. Marc Rott at the University of Wisconsin-LaCrosse who
606 used transposon mutagenesis in the teaching lab to identify genes involved in butanol oxidation
607 in *Rhodobacter sphaeroides.* We would like to thank Tim Andriese for assistance with
608 sequencing of the transposon mutant DNA and all Skovran lab members for assistance with
609 growth curves and transcriptional reporter fusion assays. TEM work was done at the Center for
610 Advanced Microscopy, Michigan State University. We would like to thank Dr. Alicia Withrow
611 for invaluable assistance with TEM experiments and Dr. Xudong Fan for his expertise using
612 TEM-EDS. E.S., N.C.M-G., P.R-J., and H.N.V. directed experiments. E.S., N.C.M-G., P.R-J.,

613 and H.N.V. wrote the manuscript. P.R-J. conducted microscopy and Ln transport experiments.
614 H.N.V, G.A.S, J.C., and E.C carried out transposon mutagenesis studies. H.N.V., G.A.S., R.C.,
615 J.C., C.R., E.M.A., E.C., N.F.L., and F.Y. constructed strains and conducted growth experiments.
616 R.C., C.H., and G.A.S. conducted expression studies. R.T.N created TransMapper.
617

618 **FUNDING SOURCES**

619 This material is based upon work supported by the National Science Foundation under Grant No.
620 1750003 and by a California State University Program for Education and Research (CSUPERB)
621 Joint Venture Grant. P.R-J. was supported by the National Science Foundation under Grant No.
622 1750003. EA and F.Y. were supported by the National Science Foundation Research Initiative
623 for Scientific Enhancement (RISE) award under Grant No. R25GM071381. F.Y. was also
624 supported by the National Institute of Health Maximizing Access to Research Careers
625 Undergraduate Student Training in Academic Research (MARC U-STAR) award under Grant
626 No. 4T34GM008253. Funding for transposon DNA isolation, PCR, and sequencing was
627 provided by San José State University through the Department of Biological Sciences.

628 **TABLES**

629 Table 1. Ability of ADH mutations to confer methanol resistance to an *fae* mutant strain on

630 succinate and methanol solid medium with La^{3+}.

Strain	Succinate + MeOH + La^{3+}
Wild type	++
fae	-
fae xoxF1	+
fae xoxF1 xoxF2	++
fae exaF	-
fae mxaF	-

631

632 Methanol is abbreviated as MeOH. No growth is represented by a - sign; growth is represented

633 with a + sign. A single + indicates that colony size is approximately half of the wild-type colony

634 size.

635 Table 2. Genes identified three or more times via transposon mutagenesis.

Gene Designation	Gene Name	Putative Function
META1_0863		LysR-type regulator
META1_1292	*cycL*	*c*-type cytochrome biogenesis
META1_1293	*cycK*	Heme lyase
META1_1294	*cycJ*	Periplasmic heme chaperone
META1_1740	*xoxF1*	Lanthanide-dependent methanol dehydrogenase
META1_1741	*xoxG*	Cytochrome *c*
META1_1742	*xoxJ*	Periplasmic binding protein
META1_1746	*orf6*	Unknown
META1_1747	*orf7*	Unknown
META1_1748	*pqqE*	PQQ biosynthesis
META1_1749	*pqqCD*	PQQ biosynthesis
META1_1750	*pqqB*	PQQ biosynthesis
META1_1771	*xoxD*	MxaD homolog
META1_1778	*lutA*	ABC transporter-periplasmic binding component
META1_1779	*lutB*	Exported protein
META1_1782	*lutE*	ABC transporter-ATP binding component
META1_1783	*lutF*	ABC transporter-membrane component
META1_1784	*lutG*	Exported protein
META1_1785	*lutH*	TonB-dependent receptor
META1_2024	*hss*	Homospermidine synthase
META1_2330	*pqqF*	Protease
META1_2331	*pqqG*	Protease
META1_2359		Fused ABC transporter
META1_2732	*ccmC*	Heme export
META1_2734	*ccmG*	*c*-type cytochrome biogenesis
META1_2825	*ccmB*	Heme export
META1_2826	*ccmA*	Heme export
META1_3908		Leucyl aminopeptidase
META1_5017		Porin family protein

636

637

638 Table 3. Growth parameters for strains grown in methanol medium with and without La^{3+}.

	Growth Rate (h^{-1})[£]	
Strain	**MeOH**	**MeOH La^{3+}**
Control strains		
Wild type	0.14 ± 0.01	0.16 ± 0.01
mxaF	NG	0.16 ± 0.01
xoxF1	30 h lag, 0.09 ± 0.01	6-9 h lag, 0.07 ± 0.00
xoxF1 xoxF2	NG*	6 h lag, 0.04 ± 0.01
mxaF xoxF1 xoxF2	NG	6 h lag, 0.04 ± 0.00
Genes involved in general methanol oxidation		
pqqBCDE	NG	NG
pqqF	NG	NG
cycK	NG	NG
ccmB	NG	NG
ccmC	NG	NG
META1_2359	NG*	NG*
mxaF META1_2359	NG	NG*
META1_3908	24 h lag, 0.05 ± 0.00	15 h lag, 0.07 ± 0.00
mxaF META1_3908	NG	15 h lag, 0.07 ± 0.01
hss	9 h lag, 0.09 ± 0.01	6 h lag, 0.10 ± 0.01
mxaF hss	NG	0.11 ± 0.01
META1_0863	0.13 ± 0.00	0.14 ± 0.00
Genes involved in Ln-dependent methanol oxidation		
xoxG	3 h lag, 0.11 ± 0.01	0.04 ± 0.00
xoxJ	21 h lag, 0.13 ± 0.00	0.04 ± 0.01
xoxD	0.14 ± 0.01	0.11 ± 0.01
mxaF xoxD	NG	6 h lag, 0.11 ± 0.01
orf6	9 h lag, 0.10 ± 0.01	0.03 ± 0.00
orf7	6 h lag, 0.14 ± 0.00	9 h lag, 0.08 ± 0.01
META1_5017	0.15 ± 0.00	0.14 ± 0.01
mxaF META1_5017	NG	21 h lag, 0.13 ± 0.01
lutA	0.15 ± 0.01	0.02 ± 0.01, 96 h; 0.08 ± 0.01[#]
mxaF lutA	NG	0.02 ± 0.00
lutB	0.15 ± 0.01	0.02 ± 0.00, 87 h; 0.03 ± 0.01[#]
mxaF lutB	NG	0.02 ± 0.00
lutC	0.13 ± 0.01	9 h lag, 0.11 ± 0.01
mxaF lutC	NG	9 h lag, 0.11 ± 0.01

Table 3. (continued)

Strain	Growth Rate (h^{-1})[£]	
	MeOH	**MeOH La^{3+}**
Genes involved in Ln-dependent methanol oxidation		
lutD	0.16 ± 0.01	0.18 ± 0.02
mxaF lutD	NG	0.16 ± 0.03
lutE	3 h lag, 0.12 ± 0.02	NG*
mxaF lutE	NG	NG*
lutF	0.12 ± 0.02	NG*
mxaF lutF	NG	NG*
lutG	12 h lag, 0.15 ± 0.01	12 h lag, 0.03 ± 0.00
mxaF lutG	NG	12 h lag, 0.03 ± 0.00
lutH	0.14 ± 0.01	0.16 ± 0.00
mxaF lutH	NG	NG*

[£]Data for a minimum of three biological replicates are reported.
* indicates if a suppressor mutation or acclimation event allowed eventual growth of the strain (detailed in Table 4).
[#] indicates two growth rates were observed with an initial growth rate lasting for the time indicated, followed by a final growth rate. The first growth rate visually appeared as a lag except strains slowly grew during this time.
NG indicates no growth. Methanol is abbreviated as MeOH.

646 Table 4. Growth parameters of suppressor and acclimation events.

Strain	MeOH		MeOH La^{3+}	
	Time of S/A (h)	**S/A Growth Rate (h^{-1}) £**	**Time of S/A (h)**	**S/A Growth Rate (h^{-1}) £**
xoxF1 xoxF2	S: 108-144	0.10 ± 0.01		
META1_2359	S: 85-100	0.11 ± 0.02	S: 85	0.10 ± 0.01
mxaF META1_2359			S: 120-140	0.07 ± 0.02
lutE			S: 75-90	0.07 ± 0.01
mxaF lutE			S: 200-220	0.02 ± 0.00
lutF			S: 79-91	0.09 ± 0.02
mxaF lutF			S: 145-157	0.02 ± 0.01
mxaF lutH			A: 90-120	0.14 ± 0.02

647 £Data for a minimum of three biological replicates is reported.
648 Abbreviations are as follows: methanol is abbreviated as MeOH, suppression as S, acclimation
649 as A.

FIGURE LEGENDS

Fig 1. Schematic representation of the metabolic processes relevant for the *mxaF fae* transposon mutagenesis study. When coordinated to Ln, the XoxF methanol dehydrogenase is known to produce formaldehyde *in vivo*. When *M. extorquens* AM1 lacks *fae* as indicated by a red X, formaldehyde accumulates to toxic levels rendering strains unable to grow on solid media even in the presence of alternative substrates such as succinate. In the absence of *mxaF*, if a process required for XoxF function is disrupted by a transposon insertion, formaldehyde is reduced or eliminated, and growth can occur using succinate as a carbon and energy source. Dashed lines are used to represent the formaldehyde transporter as this function has not been demonstrated.

Fig 2. Characterization of the Ln transport cluster. A) Genomic map of the genes contained in the Ln transport cluster (*META1_1778* to *META1_1787*). Purple, genes encoding the ABC transport system; green, gene encoding the TonB-dependent transporter; blue, genes encoding putative exported proteins identified by transposon mutagenesis; gray, lanmodulin and additional exported genes in the Ln transport cluster not identified by transposon mutagenesis. B) Schematic representation of the proteins predicted to be involved in Ln transport. The three-dimensional structures of monomers of LutH and LutA were predicted using homology modeling (HHpredserver and MODELLER) (80)and homodimers of the ABC transporter were predicted using GalaxyHomomer (81). C) Growth of wild type and *lut* mutant strains grown in 125 mM methanol medium with 2 μM $LaCl_3$. Graphs depict representative data from three biological replicates. Variation between replicates was < 5% except for *mxaF lutC* and *mxaF lutD* which had growth variances of 9 and 20% respectively as reported in Table 3.

673

674 **Fig 3. Measurement of Ln uptake.** A) Growth analysis of wild type (red circles), *lutH* encoding
675 the TonB receptor (dark blue triangles), *lutA* encoding the periplasmic binding protein
676 component of the ABC transporter (bright blue squares), *lutE* encoding the ATP binding
677 component of the ABC transporter (light blue diamonds), and *lutF* encoding the transmembrane
678 component of the ABC transporter (light blue circles), grown in the presence of limiting
679 succinate (3.75 mM), methanol (125 mM), and 2 μM $LaCl_3$. Data represent the average of three
680 biological replicates with variances < 5%. B) La^{3+} concentration (μM) present in the supernatant
681 at different optical densities (OD_{600}) for wild type (red), *lutH* (dark blue), and *lutA*, *lutE*, *lutF*
682 (gradient of light blue respectively). Each bar represents the average of three biological replicates
683 with error bars showing the standard deviation. One-way analysis of variance (ANOVA)
684 followed by a T-test was used to represent statistical significance. *The *p*-value is <0.005.

685

686 **Fig 4. Transmission and electron microscopy for visualization of Ln.** Thin sections of
687 A) *lutH*, B) *lutE* C) *lutF*, D) *lutA*, and G) wild-type strains growth in minimal medium with 3.75
688 mM succinate, 125 mM methanol, and 20 μM $LaCl_3$. White arrows indicate depositions of
689 electron scattering material in the periplasm. Each panel depicts cells that were fixed with 2.5%
690 glutaraldehyde, either post-fixed with OsO_4 and stained with uranyl acetate to detect cell
691 membranes (left subpanel), or without post-fixation and staining for elemental analysis (right
692 subpanel). E) Magnification of the La-deposits localized in the periplasmic space from the *lutA*
693 mutant strain; black arrows show the boundaries of the outer membrane and inner membrane. F)
694 Energy-dispersive X-ray analysis of the electron-dense deposits observed inside the periplasm.

695

696 **Fig 5. Assessment of the ability of an *mxaF* mutant strain to store Ln for methanol growth.**

697 Optical density (OD_{600}) measurements of cultures grown with excess $LaCl_3$ (20 μM) (gray

698 circles) until six hours post stationary phase. Cells were washed and reinoculated into La^{3+} free

699 methanol medium in La^{3+} tubes (subculture #1, dark blue circles). After 6 hours in stationary

700 phase, subculture #1 was washed and reinoculated into methanol medium without La^{3+}

701 (subculture #2, light blue circles). Representative data from three biological replicates is shown.

702 Growth variance was <5%.

703

704 **Fig 6. Visualization of Ln storage.** TEM of ultrathin sections of wild-type cells grown with (A-

705 B) and without (E-F) 20 μM La^{3+}in minimal medium with 3.75 mM succinate and 125 mM

706 methanol. C) and G) Elemental analysis of electron dense deposits was conducted using EDS on

707 unstained ultrathin sections from cells grown with (C) and without (G) La^{3+}. D) High-resolution

708 transmission electron microscopy analysis of the wild-type strain revealing the presence of an

709 atomic lattice in electron-dense areas that suggests La^{3+} is embedded in inorganic crystals inside

710 the cell.

711

712

REFERENCES

1. Chistoserdova L. 2019. New pieces to the lanthanide puzzle. Mol Microbiol 111:1127–1131.
2. Picone N, Op den Camp HJ. 2019. Role of rare earth elements in methanol oxidation. Curr Opin Chem Biol 49:39–44.
3. Skovran E, Raghuraman C, Martinez-Gomez NC. 2019. Lanthanides in Methylotrophy, p. 101–116. *In* Methylotrophs and Methylotroph Communities.
4. Pol A, Barends TRM, Dietl A, Khadem AF, Eygensteyn J, Jetten MSM, Op den Camp HJM. 2014. Rare earth metals are essential for methanotrophic life in volcanic mudpots. Environ Microbiol 16:255–264.
5. Good NM, Vu HN, Suriano CJ, Subuyuj GA, Skovran E, Martinez-Gomez NC. 2016. Pyrroloquinoline Quinone-Containing Ethanol Dehydrogenase in Methylobacterium extorquens AM1 Extends Lanthanide-Dependent Metabolism to Multi-Carbon Substrates. J Bacteriol 198:3109–3118.
6. Deng YW, Ro SY, Rosenzweig AC. 2018. Structure and function of the lanthanide-dependent methanol dehydrogenase XoxF from the methanotroph Methylomicrobium buryatense 5GB1C. J Biol Inorg Chem 23:1037–1047.
7. Lumpe H, Pol A, Op den Camp H, Daumann L. 2018. Impact of the Lanthanide Contraction on the Activity of a Lanthanide-dependent Methanol Dehydrogenase – A Kinetic and DFT Study and DFT Study. Dalt Trans 47:10463–10472.
8. Good NM, Moore RS, Suriano CJ, Martinez-Gomez NC. 2019. Contrasting in vitro and in vivo methanol oxidation activities of lanthanide-dependent alcohol dehydrogenases XoxF1 and ExaF from Methylobacterium extorquens AM1. Sci Rep 9:4248.
9. Huang J, Yu Z, Groom J, Cheng J-F, Tarver A, Yoshikuni Y, Chistoserdova L. 2019. Rare earth element alcohol dehydrogenases widely occur among globally distributed, numerically abundant and environmentally important microbes. ISME J.
10. Prejanò M, Marino T, Russo N. 2017. How Can Methanol Dehydrogenase from Methylacidiphilum fumariolicum Work with the Alien Ce III Ion in the Active Center? A Theoretical Study. Chem - A Eur J 23:8652–8657.
11. McSkimming A, Cheisson T, Carroll PJ, Schelter EJ, Roy P. 2018. Functional Synthetic Model for the Lanthanide-Dependent Quinoid Alcohol Dehydrogenase Active Site. J Am Chem Soc 140:1223–1226.
12. Keltjens JT, Pol A, Reimann J, Op Den Camp HJM. 2014. PQQ-dependent methanol dehydrogenases: Rare-earth elements make a difference. Appl Microbiol Biotechnol 98:6163–6183.
13. Akberdin IR, Collins DA, Hamilton R, Oshchepkov DY, Shukla AK, Nicora CD, Nakayasu ES, Adkins JN, Kalyuzhnaya MG. 2018. Rare Earth Elements Alter Redox Balance in Methylomicrobium alcaliphilum 20ZR. Front Microbiol 9:2735.
14. Vu HN, Subuyuj GA, Vijayakumar S, Good NM, Martinez-Gomez NC, Skovran E. 2016. Lanthanide-dependent regulation of methanol oxidation systems in Methylobacterium extorquens AM1 and their contribution to methanol growth. J Bacteriol 198:1250–1259.
15. Chu F, Beck DAC, Lidstrom ME. 2016. MxaY regulates the lanthanide-mediated methanol dehydrogenase switch in Methylomicrobium buryatense. PeerJ 4:e2435.
16. Gu W, Haque MFU, DiSpirito AA, Semrau JD. 2016. Uptake and effect of rare earth elements on gene expression in Methylosinus trichosporium OB3b. FEMS Microbiol Lett

363:pii: fnw129.
17. Masuda S, Suzuki Y, Fujitani Y, Mitsui R, Nakagawa T, Shintani M, Tani A. 2018. Lanthanide-Dependent Regulation of Methylotrophy in Methylobacterium aquaticum Strain 22A. mSphere 3:e00462-17.
18. Skovran E, Martinez-Gomez NC. 2015. Just add lanthanides. Science 348:862–863.
19. Martinez-Gomez NC, Vu HN, Skovran E. 2016. Lanthanide Chemistry: From Coordination in Chemical Complexes Shaping Our Technology to Coordination in Enzymes Shaping Bacterial Metabolism. Inorg Chem 55:10083–10089.
20. Springer AL, Morris CJ, Lidstrom ME. 1997. Molecular analysis of mxbD and mxbM, a putative sensor-regulator pair required for oxidation of methanol in Methylobacterium extorquens AM1. Microbiology 143:1737–1744.
21. Skovran E, Palmer AD, Rountree AM, Good NM, Lidstrom ME. 2011. XoxF is required for expression of methanol dehydrogenase in Methylobacterium extorquens AM1. J Bacteriol 193:6032–6038.
22. Ochsner AM, Hemmerle L, Vonderach T, Nüssli R, Bortfeld-Miller M, Hattendorf B, Vorholt JA. 2019. Use of rare-earth elements in the phyllosphere colonizer Methylobacterium extorquens PA1. Mol Microbiol 111:1152–1166.
23. Mattocks JA, Ho J V, Cotruvo JA. 2019. A Selective, Protein-Based Fluorescent Sensor with Picomolar Affinity for Rare Earth Elements. J Am Chem Soc 141:2857–2861.
24. Cotruvo, Jr. JA, Featherston ER, Mattocks JA, Ho J V., Laremore TN. 2018. Lanmodulin: A highly selective lanthanide-binding protein from a lanthanide-utilizing bacterium. J Am Chem Soc 140:15056–15061.
25. Noinaj N, Guillier M, Barnard TJ, Buchanan SK. 2010. TonB-dependent transporters: regulation, structure, and function. Annu Rev Microbiol 64:43–60.
26. Schauer K, Rodionov DA, De Reuse H. 2008. New substrates for TonB-dependent transport: do we only see the “tip of the iceberg”? Trends Biochem Sci 33:330–338.
27. Saha M, Sarkar S, Sarkar B, Kumar Sharma B, Bhattacharjee S, Tribedi P. 2016. Microbial siderophores and their potential applications: a review. Env Sci Pollut Res 23:3984– 3999.
28. Kustusch RJ, Kuehl CJ, Crosa JH. 2011. Power plays: iron transport and energy transduction in pathogenic vibrios. Biometals 24:559–566.
29. López CS, Crosa JH. 2007. Characterization of ferric-anguibactin transport in Vibrio anguillarum, p. 393–403. *In* BioMetals.
30. Fanucci GE, Cadieux N, Kadner RJ, Cafiso DS. 2003. Site-directed disulfide bonding reveals an interaction site between energy-coupling protein TonB and BtuB, the outer membrane cobalamin transporter. Proc Natl Acad Sci U S A 96:10673–10678.
31. Fanucci GE, Coggshall KA, Cadieux N, Kim M, Kadner RJ, Cafiso DS. 2003. Substrate-Induced Conformational Changes of the Perplasmic N-Terminus of an Outer-Membrane Transporter by Site-Directed Spin Labeling †. Biochemistry 42:1391–1400.
32. Jordan LD, Zhou Y, Smallwood CR, Lill Y, Ritchie K, Yip WT, Newton SM, Klebba PE. 2013. Energy-dependent motion of TonB in the Gram-negative bacterial inner membrane. Proc Natl Acad Sci 110:11553–11558.
33. Chimento DP, Mohanty AK, Kadner RJ, Wiener MC. 2003. Substrate-induced transmembrane signaling in the cobalamin transporter BtuB. Nat Struct Biol 10:394–401.
34. Neilands JB. 1995. Siderophores: Structure and Function of Microbial Iron Transport Compounds. J Biol Chem 270:26723–26726.

804 35. Imlay JA, Chin, SM, Linn S. 1988. Toxic DNA damage by hydrogen peroxide through the
805 Fenton reaction in vivo and in vitro. Science 240:640–642.
806 36. Angerer, A, Braun V. 1998. Iron regulates transcription of the Escherichia coli ferric
807 citrate transport genes directly and through the transcription initiation proteins. Arch
808 Microbiol 169:483–90.
809 37. Chen Z, Lewis KA, Shultzaberger RK, Lyakhov IG, Zheng M, Doan B, Storz G,
810 Schneider TD. 2007. Discovery of Fur binding site clusters in Escherichia coli by
811 information theory models. Nucleic Acids Res 35:6762–6777.
812 38. Griggs DW, Konisky J. 1989. Mechanism for Iron-Regulated Transcription of the
813 Escherichia coli cir Gene: Metal-Dependent Binding of Fur Protein to the Promoters. J
814 Bacteriol 171:1048–1054.
815 39. Young GM, Postle K. 1994. Repression of tonB transcription during anaerobic growth
816 requires Fur binding at the promoter and a second factor binding upstream. Mol Microbiol
817 11:943–954.
818 40. Sawyer EB, Barker PD. 2012. Continued surprises in the cytochrome c biogenesis story.
819 Protein Cell 3:405–409.
820 41. Toyama H, Inagaki H, Matsushita K, Anthony C, Adachi O. 2003. The role of the MxaD
821 protein in the respiratory chain of Methylobacterium extorquens during growth on
822 methanol. Biochim Biophys Acta 1647:372–375.
823 42. Chistoserdova L, Lidstrom ME. 1997. Molecular and mutational analysis of a DNA region
824 separating two methylotrophy gene clusters in Methylobacterium extorquens AM1.
825 Microbiology 143:1729–36.
826 43. Zheng C, Huang Y, Zhao J, Chistoserdova F. 2018. Physiological Effect of XoxG(4) on
827 Lanthanide-Dependent Methanotrophy. MBio 9:e02430-17.
828 44. Featherston ER, Rose HR, McBride MJ, Taylor E, Boal AK, Cotruvo J. 2019.
829 Biochemical and structural characterization of XoxG and XoxJ and their roles in activity
830 of the lanthanide-dependent methanol dehydrogenase, XoxF. ChemBioChem.
831 45. Versantvoort W, Pol A, Daumann LJ, Larrabee JA, Strayer AH, Jetten MSM, van Niftrik
832 L, Reimann J, Op den Camp HJM. 2019. Characterization of a novel cytochrome c as the
833 electron acceptor of XoxF-MDH in the thermoacidophilic methanotroph
834 Methylacidiphilum fumariolicum SolV. Biochim Biophys Acta - Proteins Proteomics
835 1867:595–603.
836 46. Chou H-H, Marx CJ. 2012. Optimization of gene expression through divergent mutational
837 paths. Cell Rep 1:133–140.
838 47. Daumann LJ. 2019. Essential and Ubiquitous: The Emergence of Lanthanide
839 Metallobiochemistry. Angew Chem Int Ed Engl.
840 48. Hogendoorn C, Roszczenko-Jasińska P, Martinez-Gomez NC, de Graaff J, Grassl P, Pol
841 A, Op den Camp HJM, Daumann LJ. 2018. Facile Arsenazo III-Based Assay for
842 Monitoring Rare Earth Element Depletion from Cultivation Media for Methanotrophic
843 and Methylotrophic Bacteria. Appl Environ Microbiol 84:e02887-17.
844 49. Langley S, Beveridge TJ. 1999. Effect of O-Side-Chain-Lipopolysaccharide Chemistry on
845 Metal Binding. Appl Environ Microbiol 65:489–498.
846 50. Klaus T, Joerger R, Olsson E, Granqvist C-G. 1999. Silver-based crystalline
847 nanoparticles, microbially fabricated. Proc Natl Acad Sci 96:13611–13614.
848 51. Maleke M, Valverde A, Vermeulen JG, Cason E, Gomez-Arias A, Moloantoa K, Coetsee-
849 Hugo L, Swart H, Van Heerden E, Castillo J. 2019. Biomineralization and

bioaccumulation of europium by a thermophilic metal resistant bacterium. Front Microbiol 10:1–10.

52. Leeson TS, Higgs G. 1982. Lanthanum as an intracellular stain for electron microscopy. Histochem J 14:553–60.

53. Bayer ME, Bayer MH. 1991. Lanthanide accumulation in the periplasmic space of Escherichia coli B. J Bacteriol 173:141–149.

54. Merroun ML, Ben Chekroun K, Arias JM, Gonz A Alez-Mu~ N Noz MT. 2003. Lanthanum fixation by Myxococcus xanthus: cellular location and extracellular polysaccharide observation. Chemosph 52:113–120.

55. McCulloch R, Burke ME, Sherratt DJ. 1994. Peptidase activity of Escherichia coli aminopeptidase A is not required for its role in Xer site-specific recombination. Mol Microbiol 12:241–251.

56. Krossa S, Faust A, Ober D, Scheidig AJ. 2015. Comprehensive Structural Characterization of the Bacterial Homospermidine Synthase-an Essential Enzyme of the Polyamine Metabolism. Sci Rep 6:19501.

57. Wortham BW, Patel, CN, Oliveira M. 2007. Polyamines in bacteria: pleiotropic effects yet specific mechanisms. Adv Exp Med Biol 603:106–15.

58. Schell MA. 1993. Molecular Biolgy of the LysR Family of Transcriptional Regulators. Annu Rev Microbiol 47:597–626.

59. Delaney NF, Kaczmarek ME, Ward LM, Swanson PK, Lee M-C, Marx CJ. 2013. Development of an optimized medium, strain and high-throughput culturing methods for Methylobacterium extorquens. PLoS One 8:e62957.

60. Cheng Y, Zhang L, Bian X, Zuo H, Dong H. 2018. Adsorption and mineralization of REE-lanthanum onto bacterial cell surface. Env Sci Pollut Res 25:22334–22339.

61. Mullen MD, Wolf DC, Ferris FG, Beveridge TJ, Flemming CA, Bailey3 GW. 1989. Bacterial Sorption of Heavy Metals. Appl Environ Microbiol 55:3143–3149.

62. Zhan G, Li D, Liang Zhang &. 2012. Aerobic bioreduction of nickel(II) to elemental nickel with concomitant biomineralization. Appl Microbiol Biotechnol 96:273– 281.

63. Bai HJ, Zhang ZM, Guo Y, Yang GE. 2009. Biosynthesis of cadmium sulfide nanoparticles by photosynthetic bacteria Rhodopseudomonas palustris. Colloids Surfaces B Biointerfaces 70:142–146.

64. Sousa T, Chung A-P, Pereira A, Piedade AP, Morais P V. 2013. Aerobic uranium immobilization by Rhodanobacter A2-61 through formation of intracellular uranium-phosphate complexes. Metallomics 5:390–397.

65. Couradeau E, Benzerara K, Gérard E, Moreira D, Bernard S, Brown GE, López-García P. 2012. An Early-Branching Microbialite Cyanobacterium Forms Intracellular Carbonates. Science 336:459–462.

66. Debieux CM, Dridge EJ, Mueller CM, Splatt P, Paszkiewicz K, Knight I, Florance H, Love J, Titball RW, Lewis RJ, Richardson DJ, Butler CS. 2011. A bacterial process for selenium nanosphere assembly. Proc Natl Acad Sci 108:13480–13485.

67. Rahn-Lee L, Komeili A. 2013. The magnetosome model: Insights into the mechanisms of bacterial biomineralization. Front Microbiol 4:352.

68. Kulaev I. 1979. The Biochemistry of Inorganic Polyphosphates. John Wiley & Sons Ltd.

69. Friedberg I, Avigad G. 1968. Structures containing polyphosphate in Micrococcus lysodeikticus. J Bacteriol 96:544–553.

70. Pallerla SR, Knebel S, Polen T, Klauth P, Hollender J, Wendisch VF, Schoberth SM.

2005. Formation of volutin granules in Corynebacterium glutamicum. FEMS Microbiol Lett 243:133–140.

71. Widra A. 1959. Metachromatic granules of microorganisms. J Bacteriol 78:664–670.
72. Bertani G. 1951. Studies on lysogenesis. I. The mode of phage liberation by lysogenic Escherichia coli. J Bacteriol 62:293–300.
73. Marx CJ. 2008. Development of a broad-host-range sacB-based vector for unmarked allelic exchange. BMC Res Notes 1:1.
74. Marx CJ, Lidstrom ME. 2002. Broad-host-range cre-lox system for antibiotic marker recycling in Gram-negative bacteria. Biotechniques 33:1062–1067.
75. Simon, R. U. P. A. P., Priefer, U., & Pühler A, Simon R, Priefer U, Pühler A. 1983. A broad host range mobilization system for in vivo genetic engineering: transposon mutagenesis in gram negative bacteria. Nat Biotechnol 1:784–791.
76. Jacobs MA, Alwood A, Thaipisuttikul I, Spencer D, Haugen E, Ernst S, Will O, Kaul R, Raymond C, Levy R, Chun-Rong L, Guenthner D, Bovee D, Olson M V., Manoil C. 2003. Comprehensive transposon mutant library of Pseudomonas aeruginosa. Proc Natl Acad Sci 100:14339–14344.
77. Marx CJ, O'Brien BN, Breezee J, Lidstrom ME. 2003. Novel methylotrophy genes of Methylobacterium extorquens AM1 identified by using transposon mutagenesis including a putative dihydromethanopterin reductase. J Bacteriol 185:669–673.
78. Manoil C, Traxler B. 2000. Insertion of In-frame Sequence Tags into Proteins Using Transposons. Methods 20:55–61.
79. Nagai T, Ibata K, Park ES, Kubota M, Mikoshiba K, Miyawaki A. 2002. A variant of yellow fluorescent protein with fast and efficient maturation for cell-biological applications. Nat Biotechnol 20:87–90.
80. Söding J, Biegert A, Lupas AN. 2005. The HHpred interactive server for protein homology detection and structure prediction. Nucleic Acids Res 33:W244–W248.
81. Baek M, Park T, Heo L, Park C, Seok C. 2017. GalaxyHomomer: A web server for protein homo-oligomer structure prediction from a monomer sequence or structure. Nucleic Acids Res 45:W320–W324.

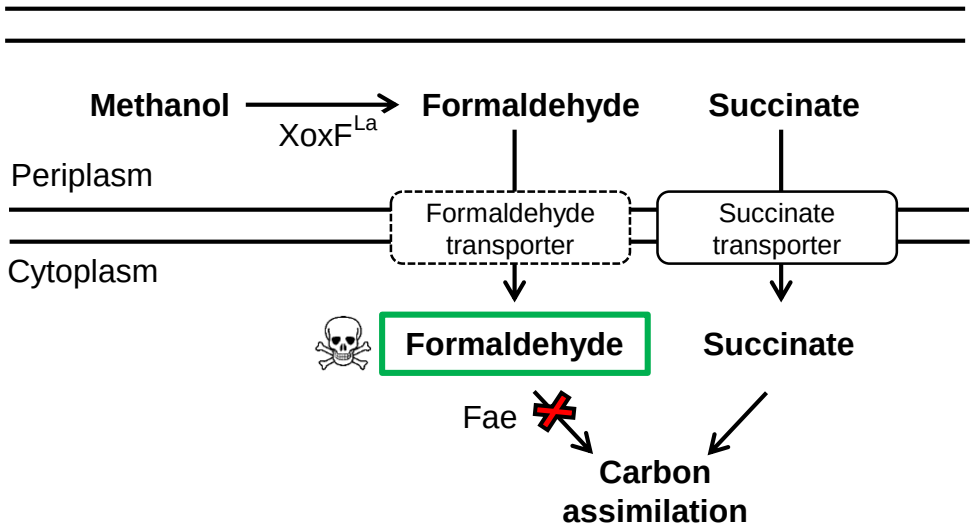
Methanol
XoxF^La
Formaldehyde
Succinate
Periplasm
Formaldehyde transporter
Succinate transporter
Cytoplasm
Formaldehyde
Succinate
Fae
Carbon assimilation

A

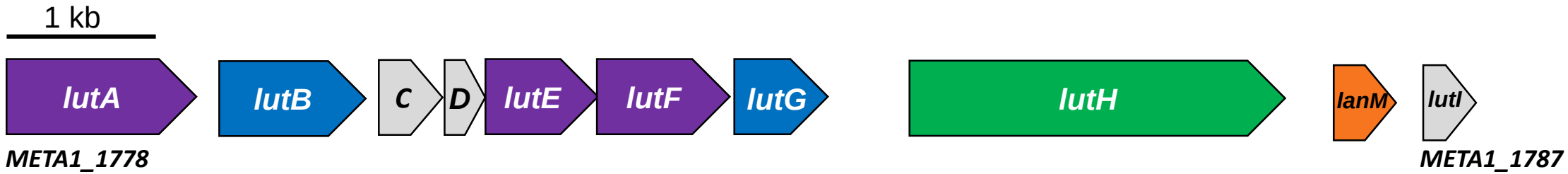
1 kb
lutA
lutB
C
D
lutE
lutF
lutG
lutH
lanM
lutI
META1_1778
META1_1787

B

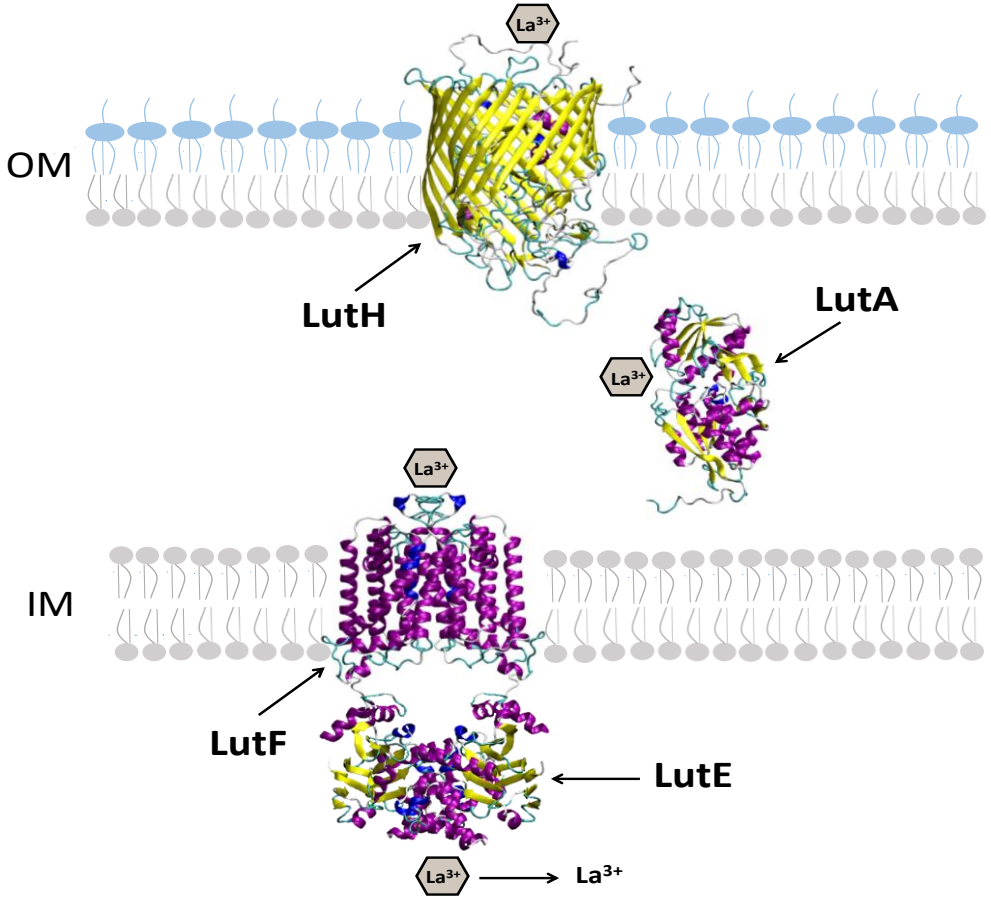
La3+
OM
LutH
LutA
IM
LutF
LutE
La3+ → La3+

C

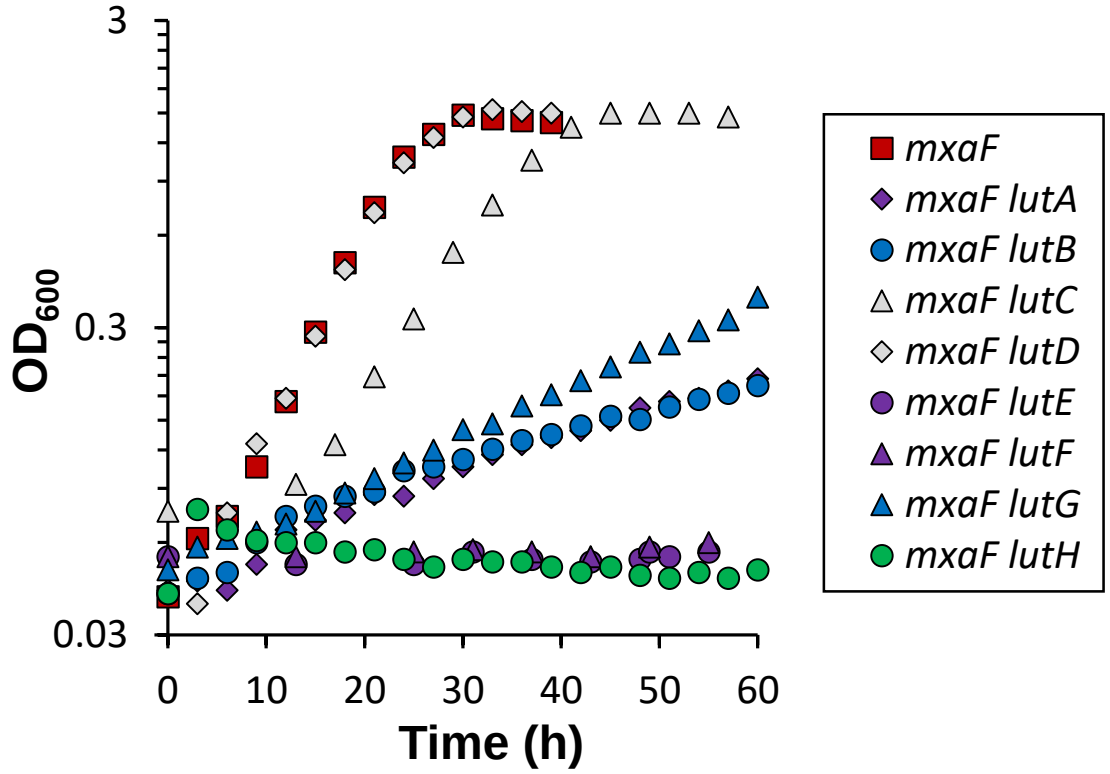
3
0.3
0.03
OD600
0
10
20
30
40
50
60
Time (h)
mxaF
mxaF lutA
mxaF lutB
mxaF lutC
mxaF lutD
mxaF lutE
mxaF lutF
mxaF lutG
mxaF lutH

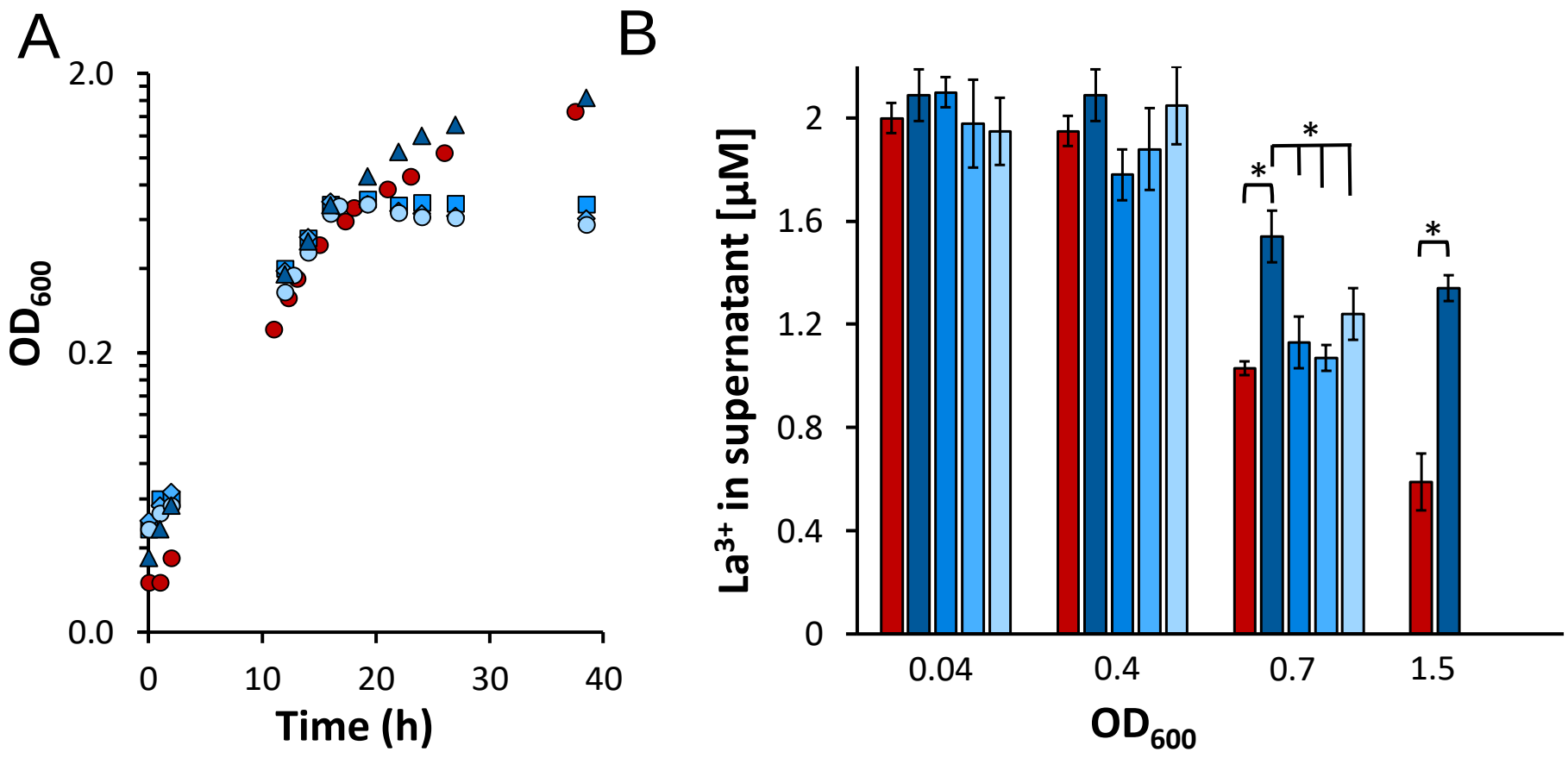
A
2.0
0.2
0.0
OD600
0
10
20
30
40
Time (h)
B
La3+ in supernatant [µM]
2
1.6
1.2
0.8
0.4
0
*
*
*
0.04
0.4
0.7
1.5
OD600

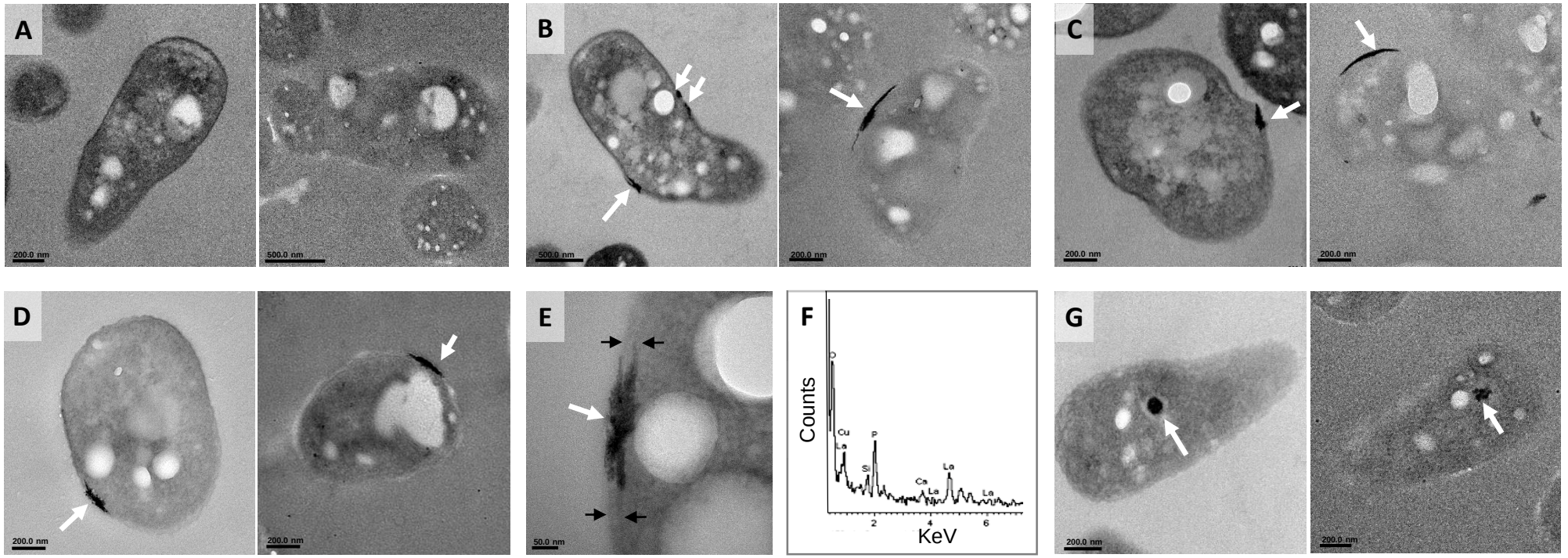
A
200.0 nm
500.0 nm
B
500.0 nm
200.0 nm
C
200.0 nm
200.0 nm
D
200.0 nm
200.0 nm
E
50.0 nm
F
Counts
KeV
O
Cu
La
P
Si
Ca
La
La
La
2
4
6
G
200.0 nm
200.0 nm

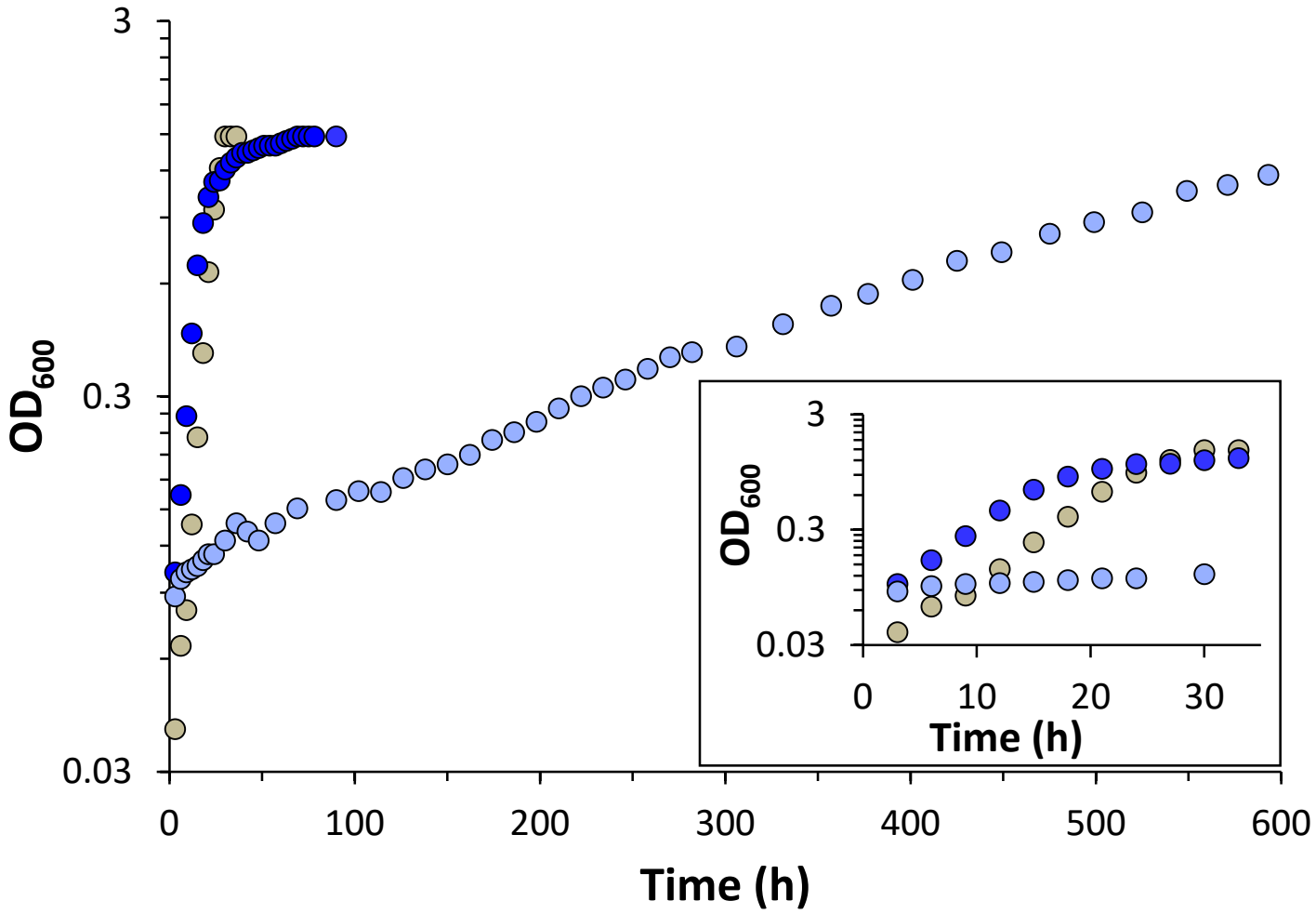
3
0.3
0.03
OD600
0
100
200
300
400
500
600
Time (h)
3
0.3
0.03
OD600
0
10
20
30
Time (h)

+ La^{3+}

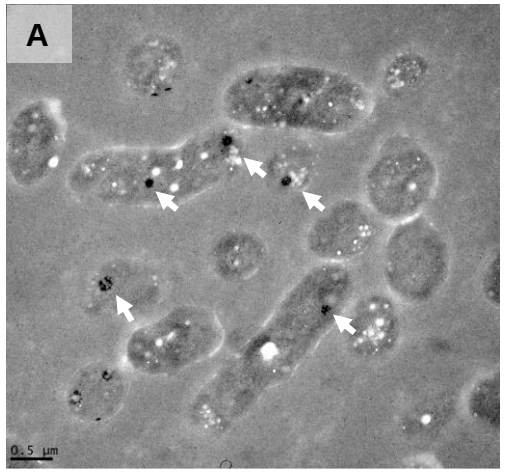
A
0.5 µm

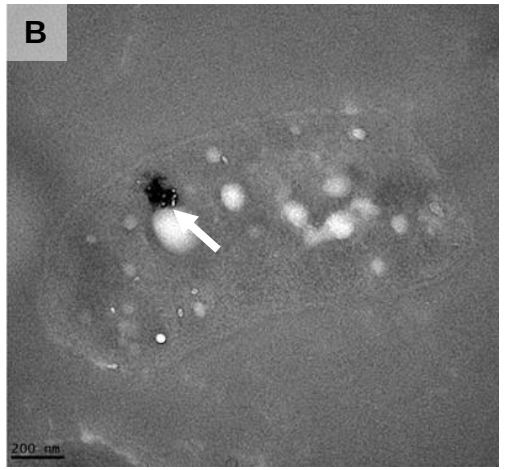
B
200 nm

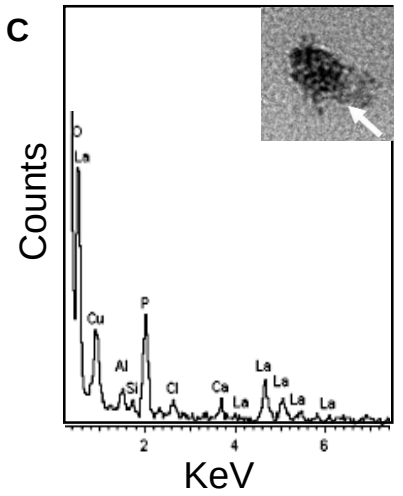
C
Counts
O
La
Cu
P
Al
Si
Cl
Ca
La
La
La
La
2
4
6
KeV

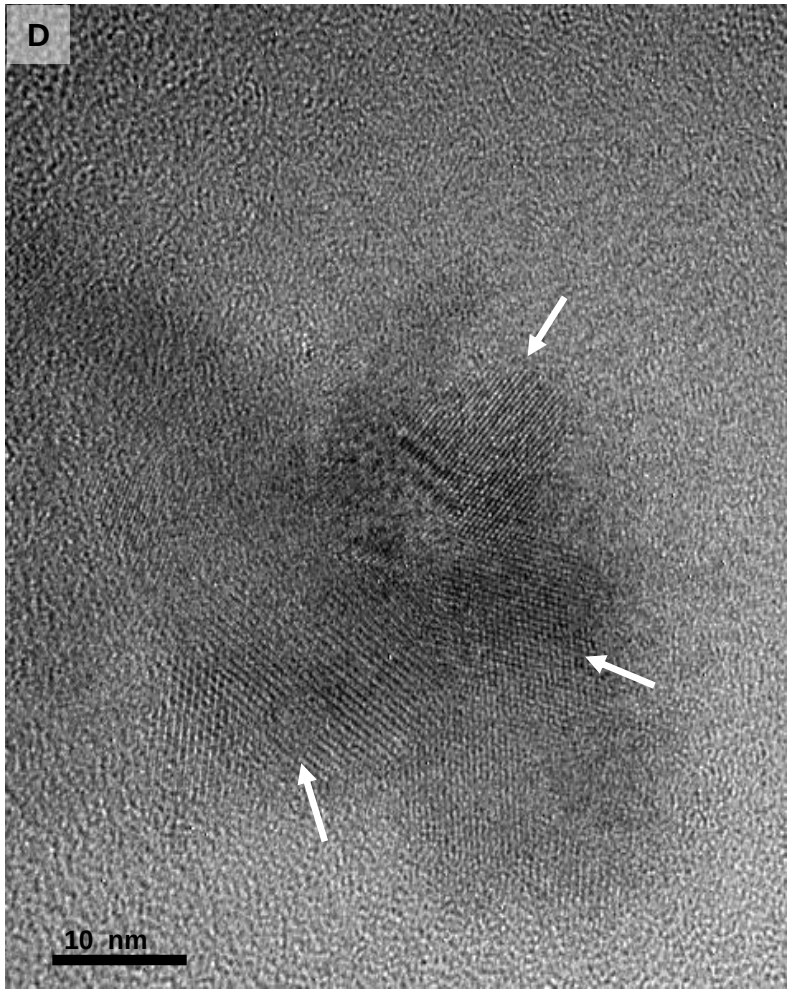
D
10 nm

No La^{3+}

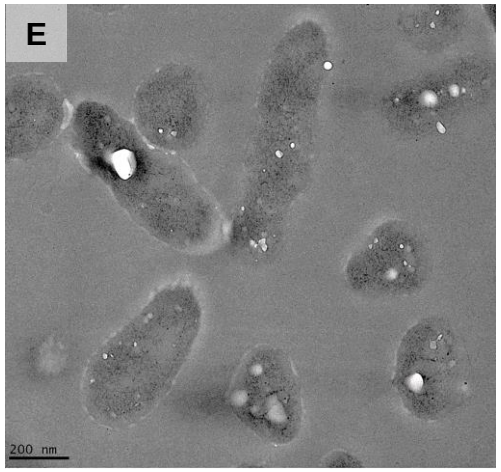
E
200 nm

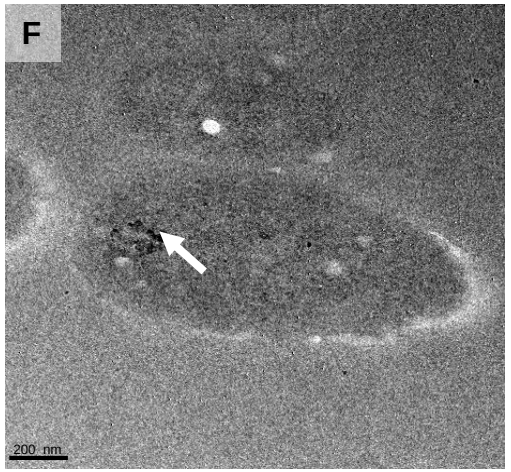
F
200 nm

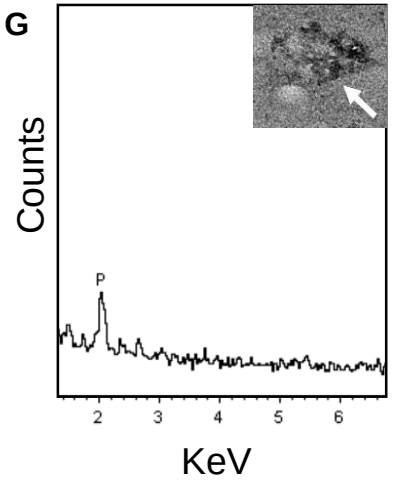
G
Counts
P
2
3
4
5
6
KeV